

# How the QCD trace anomaly behaves at the core of twin stars?

José C. JIMÉNEZ,<sup>1,2</sup> Lucas LAZZARI,<sup>3</sup> and Victor P. GONÇALVES<sup>3,4</sup>

<sup>1</sup>*Departament of Astrophysics, Brazilian Center for Research in Physics (CBPF),  
Rua Dr. Xavier Sigaud, 150, URCA, Rio de Janeiro CEP 22210-180, RJ, Brazil*

<sup>2</sup>*Universidad Tecnológica del Perú, Arequipa - Perú*

<sup>3</sup>*Institute of Physics and Mathematics, Federal University of Pelotas,  
Postal Code 354, 96010-900, Pelotas, RS, Brazil*

<sup>4</sup>*Institute of Modern Physics, Chinese Academy of Sciences, Lanzhou 730000, China*

(Dated: August 22, 2024)

We investigate the behavior of the dense and cold (normalized) QCD trace anomaly,  $\Delta$ , in the interior of twin neutron stars (obtained from several sets of equations of state in agreement with modern compact-star and multimessenger data) satisfying static and dynamic stability conditions. We scan this parameter space in order to look for effects caused by the presence of a strong first-order phase transition connecting hadron and quark phases by means of a Maxwell construction. We found robustly that  $\Delta$  suffers an abrupt decrease around the transition point, even reaching large negative values ( $\Delta \simeq -0.35$ ), in marked contrast to current studies pointing out a smooth behavior with  $\Delta \gtrsim 0$  at all densities. Besides, we characterize the behavior of conformal factor,  $d_c$ , in twin stars for which we perform comparisons with theoretical constraints, e.g. from Bayesian studies adjusted to agree with pQCD. All this allows us to infer and hypothesize modifications in the strong QCD coupling in dense nuclear matter with a strong thermodynamic discontinuity.

## I. INTRODUCTION

According to the Standard Model of Particle Physics, every observable concerning strong nuclear interactions should be derivable from Quantum Chromodynamics (QCD) having two main (poorly understood) aspects: color confinement and chiral symmetry breaking ( $\chi$ SB) [1]. In order to probe them, one would need a reliable knowledge (at some fiducial scale) of the strong coupling  $\alpha_s$  and the bare quark masses for the active flavors [1]. Currently, we have only a theoretical control on QCD at high energies due to *asymptotic freedom*, i.e.  $\alpha_s \ll 1$ , thus allowing us to characterize it as a chirally symmetric and deconfined QCD phase, altogether called perturbative QCD (pQCD) [1]. Nevertheless, at hadronic energies, the QCD coupling increases to a non-small value ( $\alpha_s \sim 1$ ), thus making extremely difficult studying non-perturbative  $\chi$ SB and (de)confinement [1].

Although there are remarkable advancements towards probing these non-perturbative features of QCD vacuum in collider physics, e.g. the LHC at CERN (see, e.g., Ref. [2]), its emergent thermodynamic observables at equilibrium<sup>1</sup> to probe relevant regimes, e.g. its equation of state (EoS), are still not well understood [4]. For instance, lattice QCD (LQCD) only provides reliable results for hot QCD matter [5, 6] with background magnetic [7, 8] and electric fields [9] or finite isospin densities [10, 11], all of them being of relevance for heavy-ion physics. Nevertheless, most strongly interacting matter in the Universe is baryonic, being the extreme density situation present at the core of heavy neutron stars (NS), where a deconfinement transition is possible at  $T = 0$  [12]. Unfortunately,

the LQCD method to finite baryon densities is strictly forbidden by the sign problem [13].

To alleviate this difficulty at finite baryochemical potentials,  $\mu_B$ , available NS data (related to their mass-radius ( $M-R$ ) diagram [14–18] and tidal deformabilities from binary NS mergers [19]) is currently employed to constrain the behavior of the NS EoS at intermediate (non - perturbative) densities (see, e.g., [20]). Broadly, their approach consists in interpolating theoretical results between the extreme cases of low and high  $\mu_B$ , i.e. chiral effective theory (CET) [21] and pQCD [22], respectively. After that, the outcomes are adjusted to respect astrophysics and experimental nuclear data, thermodynamic consistency and causality limits [23].

While one might be tempted to believe that the physics of (de)confinement and  $\chi$ SB are hidden within these continuous interpolations (as occurs when using heavy-ion data to constrain the baryon-free QCD EoS at  $T \neq 0$  remarkably coinciding in most cases with the corresponding LQCD results [24]), most of these studies mainly favor smooth EoSs at all densities (e.g. see also Ref. [25]). They also point out that the (adiabatic) speed of sound,  $c_s^2 \equiv dP/d\epsilon$  (being ‘ $\epsilon$ ’ the energy density and ‘ $P$ ’ the pressure), of dense and cold QCD matter surpasses the conformal bound,  $c_s^2 = 1/3$ , in the non - perturbative sector of baryon densities, even reaching values near the causality limit,  $c_s^2 = 1$  [26], something which is in tension with field theory studies [27, 28]. Furthermore, Ref. [29] even suggest the presence of quark matter (QM) in some maximal-mass NSs if  $c_s^2 \gtrsim 0.5$ . It should be noticed that the above findings have received support from agnostic Bayesian studies [30, 31].

In this sense, along the last few years, great attention was given to get insights for this large values of  $c_s^2$  and verify if it is a realistic property of dense matter or only an artificial effect required to make sense of the

<sup>1</sup> The non-equilibrium situation concerning transport properties is even far more complex. See, e.g. Ref. [3] and references therein.

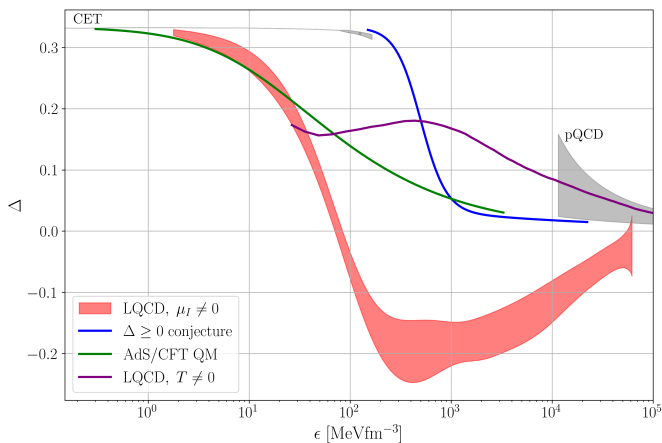


FIG. 1. Behavior of the normalized in-medium trace anomaly vs energy density ( $\Delta$  vs  $\epsilon$ ) for QCD matter in different extreme conditions. In particular, we display known findings for i) the conjectured positiveness of Ref. [33] based upon the maximum mass bound of NSs ( $\Delta \geq 0$  conjecture), ii) AdS/CFT QM [34] (see Appendix A), iii) baryon-free LQCD at finite temperatures (LQCD,  $T \neq 0$ ) [5, 6] and iv) LQCD for cold isospin matter (LQCD,  $\mu_I \neq 0$ ) [11]. We superimposed them in the same plot to clearly show their sign differences. Note that the bands CET and pQCD are only given for  $\mu_B \neq 0$ .

employed (agnostic or not) interpolations [32]. Among these investigations, the work of Ref. [33] had taken a different path by connecting  $c_s^2$  to the so-called (normalized) dense QCD *trace anomaly*  $\Delta \sim \epsilon - 3P$  (to be fully defined in Sec. III) which, broadly, is a measure of the quantum breaking of scale-conformal invariance<sup>2</sup>. This work (based on modern NS data) and other past studies (from e.g. baryon-free LQCD [5, 6] at all temperatures, pQCD with CET [33] at their range of validity, and holographic AdS/CFT results [34]) concerning  $\Delta$  conjecture its positivity at all densities. On the other hand, isospin LQCD found  $\Delta < 0$  for a large range of intermediate densities, i.e. its non-perturbative region [10, 11]. In fact, Ref. [11] indicate that their large negative  $\Delta$  is mostly caused by a pairing term (akin to the CFL phase of QM). We display the behavior of these cited results in Fig. 1.

Thus, from the pure definition of  $\Delta$ , there is no general criterium (like a non-perturbative QCD theorem) preventing us from getting a negative behavior at intermediate  $\mu_B$  since it depends on the interactions introduced in the Lagrangian defining the Landau thermodynamic potential [4]. For instance, it can be proven [35] that for pure electromagnetic interactions, one has  $\Delta \geq 0$ . However, it has also been proven within the NJL and leading-order CEF [36] that at  $T = 0$  and finite isospin densities, a transition from  $\Delta \geq 0$  to  $\Delta < 0$  occurs, pos-

sibly corresponding to a BEC-BCS crossover. Besides, a negative  $\Delta$  at  $T \neq 0$  in the primordial universe for pion condensation [37] had been found, being correlated to both large  $c_s^2$  and leptonic densities.

For heavy-ion matter ( $T \neq 0$  and  $\mu_B \lesssim T$ ), pQCD reaches its conformal limit at very high temperatures, i.e.  $\Delta \rightarrow 0$ . However, at intermediate ones, there is no clear explanation for this phenomenon within QCD. In fact, up to now, there exist few favorable findings for this trend, e.g. Ref. [38]. In particular, this issue was studied in Ref. [39] at  $T \neq 0$  from a hydrodynamic perspective relating the QCD bulk viscosity,  $\zeta_{\text{QCD}}$ , and the (unnormalized) trace anomaly, i.e.  $\zeta_{\text{QCD}} \sim \Delta$ , stating that (at least partially) it should be always be positive<sup>3</sup> in QCD in order to truly represent a dissipative term [40].

For NS matter ( $\mu_B \neq 0$  and  $T \ll \mu_B$ ), some simple models studied this observable, e.g. Ref. [41] found that the expectation of  $\Delta \geq 0$  is violated even while keeping Lorentz invariance. Within their context, this happens because the short-range repulsion of the effective nuclear interactions tend to very rapidly stiffen the EoS at high densities. Unfortunately, their conclusion depends on the nonexistence of a change of matter phase. Nevertheless, in principle, strongly-discontinuous phase transitions might arise in dense QCD matter due to: i) generic arguments against the Schaefer-Wilczek conjecture (for a smooth hadron-quark continuity) posing the necessity of a discontinuous transition [42, 43], ii) potential effects from non-perturbative Gribov-Swanziger-like models for dense matter already favoring  $\Delta < 0$  in SU(2) at intermediate  $T$  [44], iii) the activation-decoupling [45, 46] of hadronic and/or quark degrees of freedom (affecting  $\alpha_s$ ) around the transition point, iv) the “hidden” pseudo-conformal QCD symmetry yet to be better understood when changing phases [47], among other works [48–50].

In order to probe this kind of dense matter, one might employ twin NSs [51] which are unique stellar objects satisfying those strong-discontinuity requirements. Unfortunately, within the (Bayesian or not) interpolation approach, there are currently few EoS studies (see, e.g. Refs. [52–54]) dealing with this possibility for which they mainly conclude that it is very unlikely for this type of discontinuities to occur. Other related works (Refs. [55–57] from NS hydrostatic observables and Refs. [58, 59] from fully dynamical NS mergers), point out that it is too early to dismiss this intriguing possibility which only an *ab initio* non-perturbative approach might conclusively discard or not (see, e.g., Ref. [60] applying quantum computing to dense LQCD).

<sup>3</sup> Explicitly [39]

$$\zeta_{\text{QCD}} = \frac{1}{\omega_0} \left\{ T^5 \frac{\partial}{\partial T} \left( \frac{\epsilon - 3P}{T^4} \right)_{\text{LQCD}} + 16|\epsilon_v| \right\},$$

where  $\omega_0 = \omega_0(T) \sim T$  are the zero-mode Matsubara frequencies of hot pQCD and  $\epsilon_v < 0$  is the vacuum energy density which can be, e.g. the bag constant of the MIT model.

<sup>2</sup> It is also known as the ‘QCD interaction measure’ at finite temperatures. As we will see below, this is not appropriate since it assumes its positiveness which, in general, is not always the case.

Thus, it is necessary a comprehensive study of the behavior of  $\Delta$  when strong discontinuities are present, which for us the perfect astrolaboratory will be twin stars. As far as we know, the only work studying a little bit about  $\Delta$  in twin stars (in the context of modified theories of gravity) was that of Ref. [61], although their findings pointed out to slightly negative values (maximally reaching  $\Delta \approx -0.1$ , a value which was also considered in the work of Ref. [33]) without proving the radial stability of their stars nor gravity-independent inference of  $\Delta$ . Apart from that work, only Refs. [62–64] investigated  $\Delta$  in some detail for a generic set of hybrid NS EoSs with continuous transitions finding  $\Delta \gtrsim 0$  connected to their maximal  $c_s^2$  ( $\sim 0.8$ ). Notice that their assumption of slightly negative  $\Delta$  was reached monotonically (without restriction due to a possible change of phases) approaching very slowly  $\Delta \rightarrow 0$  to agree with pQCD.

Furthermore, Refs. [65, 66] and [67] studied rigorously through the Bayesian and deep-neural networks viewpoints, respectively, the effects of a first-order phase transition in NS observables adjusted to agree with up-to-date astrophysics constraints. In particular, their findings indicate again that  $\Delta$  is almost always positive, except within a small energy-density region which favors slight  $\Delta < 0$  although smoothly [65] (or discontinuously [66, 67]) approaching (or not) pQCD at high densities. Unfortunately, no robust/clear explanation for this behavior is given and, in fact, Ref. [66] even employs the  $\Delta > 0$  conjecture to reduce their parameter space. Moreover, the quite recent work of Ref. [68] attempts to probe the effects of a first-order transition on  $\Delta$ , the transition having strength (jumps in  $\Delta\epsilon$ ) depending upon the maximal Bayesian-inference thickness in ‘ $\epsilon$ ’ of their EoS band, which in practice is not large enough to produce twin stars with its novel implications for  $\Delta$ , as we do here.

In the present work, we shall focus our attention on the behavior of the normalized trace anomaly,  $\Delta$ , in cold/dense matter suffering a strong discontinuous phase transition producing twin NSs in a large parameter space. The paper is organized as follows. In Secs. II, III we explain the main ideas behind twin stars, i.e. hydrostatic and dynamical conditions for their existence, EoSs and behavior of  $\Delta$  with discontinuous transitions. Section IV presents our robust findings for  $\Delta$  within the distinct categories of studied twin stars. Rapid and slow conversions are also considered when characterizing the sign of  $\Delta$ . In Sec. V we give analytical discussions for our numerical findings in Sec. IV to get insights for the appearance of negative  $\Delta$  around the transition point. Section VI presents our conclusions and outlook. Additional discussions are presented in five Appendixes.

## II. TWIN-STAR ESSENTIALS

Along this section we point out the basic static and dynamic conditions leading to fully stable twin neutron stars, i.e. the stringent Seidov’s criterium and stability

of the radial zero-mode with rapid/slow junction conditions, respectively. In practice, these conditions will serve us to properly choose the parameters in our EoSs for the hadronic and quark phases, which in turn adjust the behavior of the normalized trace anomaly,  $\Delta$ .

### A. SEIDOV CRITERIUM AND TWIN-STAR MATTER

As usual, twin NSs families are determined from a matching between a hadronic EoS (e.g. coming from CET satisfying low-density nuclear data) up to a transitional pressure,  $P_t$ , from which a QM EoS begins through a strongly discontinuous phase transition, both phases connected by a Maxwell or Gibbs construction [12]. Besides, at the transition point, the energy and baryon number densities present large jumps ( $\Delta\epsilon$  and  $\Delta n_B$ , respectively) due to the aforementioned 1st-order transition, manifested through a finite value of latent heat  $Q \equiv \epsilon_Q^{\min} - \epsilon_H^{\max} = \mu_c \Delta n_B$  (being ‘ $\mu_c$ ’ the critical baryochemical potential, ‘ $\epsilon_Q^{\min}$ ’ the minimum value of energy density for the QM phase, and ‘ $\epsilon_H^{\max}$ ’ the maximum value reached by the hadronic phase). Besides, it should always be kept in mind that only a delicate matching of a stiff hadronic EoSs to a stiff QM one ( $c_s^2 > 1/3$ ) favors the existence of these third-branch of hybrid NSs [45, 48, 51].

**Seidov criterium:** For twin stars to exist, they must satisfy the Seidov criterion [51], which establishes the critical value in the energy density jump,  $\Delta\epsilon_{\text{crit}}$ , in the sense that for smaller values, the hybrid and hadronic branches are connected, and no twin stars are possible. This criterion can be expressed as [51]

$$\Delta\epsilon \geq \Delta\epsilon_{\text{crit}} \equiv \frac{1}{2}\epsilon_t + \frac{3}{2}P_t, \quad (1)$$

being ‘ $\epsilon_t$ ’ the onset energy density for the phase transition to occur (which below we will interpret as  $\epsilon_t \equiv \epsilon_H^{\max}$ ). Thus, Eq. (1) ensures the presence of an unstable branch in the  $M$ – $R$  diagram, giving rise later to the ultradense and stable branch *twin stars* at high densities. We now model their hybrid twin-star EoSs.

**Parameters at the transition point:** Our twin EoSs will have  $P_t$ ’s in the range [10, 100] MeVfm<sup>−3</sup> for which we computed  $\Delta\epsilon$  and varied it between 1.1 and 10 times its initial value. Since twin stars require a stiff QM EoS, we probe two high values for its respective  $c_s^2$ , the first  $c_s^2 = 1$  and the second  $c_s^2 = 0.5$ . Notice that both are non-conformal, one even reaching the causality limit.

**Hadronic phase:** It is conveniently (from a numerical viewpoint) described by the generalized piecewise polytropes (GPP) [69] that consistently assure continuity of the pressure, energy density and their derivatives. For the outer crust, we use the GPP form of the SLy4 (as presented in Table III of Ref. [69]). For densities larger than  $1.1n_0$  (being  $n_0 = 0.16$  fm<sup>−3</sup> the saturation density), we will assume a model agnostic GPP that connects with the stiffest CEF EoS [70, 71]. In order to achieve this,

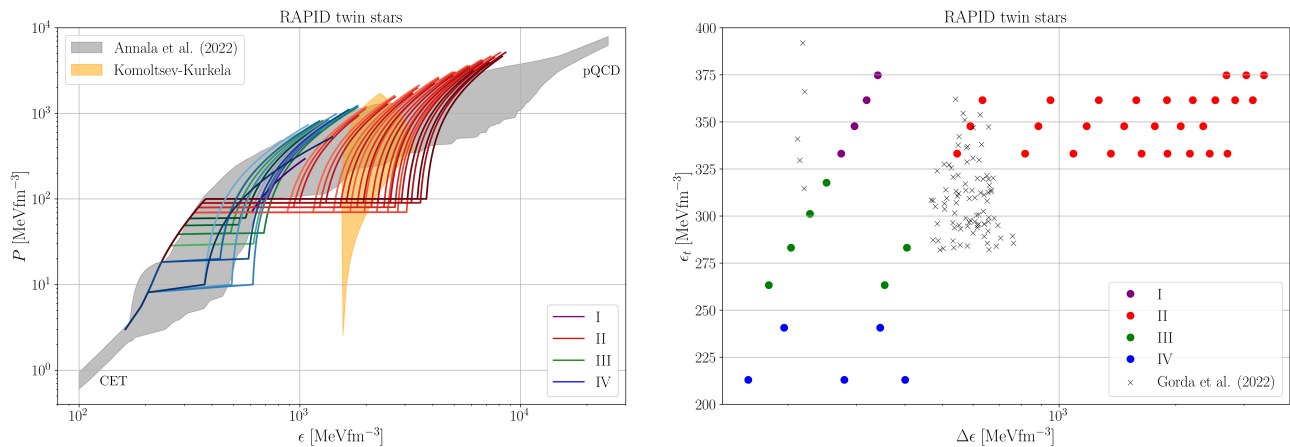


FIG. 2. Family of EoSs (*left panel*) and corresponding Seidov's parameter space (*right panel*) for Category I-IV stable twin stars with rapid conversions. For comparison, we also display (*left panel*) results from CET [21] and pQCD [22] as well as the astrophysics-constrained band (grey) of EoSs at intermediate densities of Annala et al. [20] and pQCD constraint (orange band) of Komoltsev-Kurkela [74] in the high- $n_B$  limit. Besides, the symbols 'x' (*right panel*) represent the findings of Ref. [55].

our model agnostic GPP has the following parameters:  $\log_{10}[\rho_0/(\text{g cm}^{-3})] = 13.865$ ,  $\log_{10} K_1 = -27.22$ ,  $\Gamma_1 = 2.77$ ,  $\Gamma_2 = 7.0$  and  $\Gamma_3 = 3.0$ . For the other two dividing densities, we have used  $\log_{10}[\rho_1/(\text{g cm}^{-3})] = 14.45$  and  $\log_{10}[\rho_2/(\text{g cm}^{-3})] = 14.58$ . It is worth to stress at this point, that in Appendix D we display our findings for  $\Delta$  employing the so-called *intermediate* CET of Ref. [21] in order to probe the robustness of our conclusions.

**Quark phase:** For this high-density sector of the twin EoS, we employ the well known constant-speed-of-sound (CSS) parametrization [72], which allows the description of the hybrid EoS through a set of three parameters:  $P_t$ ,  $\Delta\epsilon$  and constant  $c_{s,Q}^2$ , i.e.  $c_{s,Q}^2 \equiv s$ . In this manner, the full hybrid EoS is written as (with Maxwell construction)

$$\epsilon(P) = \begin{cases} \epsilon_H(P) & P < P_t, \\ \epsilon_H(P_t) + \Delta\epsilon + s^{-1}(P - P_t) & P > P_t. \end{cases} \quad (2)$$

For illustrative purposes, we present in Table I some particular values for these needed parameters to construct a CSS EoS for twin stars and estimate their magnitudes. For this, we follow the classification of Ref. [73] (see also references therein) of four types of twins depending basically on the combination of maximal masses obtained for the hadronic and twin branches within each category, i.e. Category I: the hadronic and twin maximums exceed the  $2M_\odot$  limit, Category II: only the hadronic maximum reaches the  $2M_\odot$  limit, Category III: the maximum of the hadronic branch lies in the range  $[1, 2]M_\odot$  while the twin maximum exceeds  $2M_\odot$ , and Category IV: the twin maximum exceeds the  $2M_\odot$  limit but the maximum of the hadronic branch appears below  $1M_\odot$ .

In the left panel of Fig. 2, we present (in different colors) our employed twin EoSs for each category along this work. Being more specific, in the next subsection, we will classify two types of twins depending on their stability against radial pulsations: the rapid and slow con-

Category	$\epsilon_H^{\max} = \epsilon_t$	$\epsilon_Q^{\min}$	$P_t$	$\Delta\epsilon$	$c_s^2$
I	333.08	607.34	70	274	1
II	333.08	878.88	70	545	1
III	263.73	441.62	30	178	1
IV	212.91	370.85	10	157	1

TABLE I. Sample of parameters used in this work for the CSS parametrization. All they are in  $\text{MeV fm}^{-3}$  while the speed of sound is in units of the speed of light.

versions. In turn, this allows us to construct hundreds of twin EoSs which unfortunately might obscure the visual analysis of their behavior. Thus, without loss of generality, we chose to display only the results for the rapid case which as a whole is a somewhat smaller set compared to the slow twin stars whose EoSs overlap several times and imposes visual challenges for the analysis. In particular, when compared with the broad (only adjusted to produce NSs with masses higher than  $2M_\odot$  and the GW170817 tidal deformability limit) grey band of EoSs of Annala et al. [20] (containing also results for the extreme opposite limits of CET and pQCD) which for us it will represent a benchmark NS EoS, where it was not explicitly considered the possibility of a first-order transition for their intermediate-density interpolations.

Besides, in this same panel, we put the orange band of Komoltsev-Kurkela [74] which is a region of pressures/energy densities, which can be consistently (from the thermodynamic viewpoint) and very generically (any reasonable smooth curve) above  $10n_0$ , but forced to converge to pQCD at  $40n_0$ . In practice, if our twin EoS pass through the orange band, we have some certainty of expecting that our EoSs will reach pQCD at  $40n_0$ . On the other hand, although the study of Komoltsev-Kurkela considered also potential first-order transitions, they maximally focused on the behavior of the NS EoS

at  $10n_0$ . Nevertheless, one can clearly see in the left panel of Fig. 2 that Categories I and II lie at even higher densities (around  $10 - 30n_0$ ), thus leading us to believe that the work of Komoltsev-Kurkela should be extended to the twin-star extreme densities in the region  $10 \leq n_B/n_0 \leq 30$ . Interestingly, Categories III and IV fit very well to the band of Annala et al. [20]. Now, in the right panel of Fig. 2, we present a comparison of our parameter space of the left panel (satisfying Eq. 1) with the one from [55], where we show the energy density at the transition point  $\epsilon_t$  as a function of  $\Delta\epsilon$ . Basically, our values for the  $\Delta\epsilon$ 's of Category II are significantly larger than those in Ref. [55].

## B. STABLE TWIN STARS: RAPID AND SLOW CONVERSIONS

**Hydrostatic equilibrium:** Twin stars are interpreted as solutions of the Tolman-Oppenheimer-Volkov (TOV) equations ( $G = c = 1$ ) which determine the structural properties of spherical compact stars. They are [12]

$$\frac{dP}{dr} = -\frac{\epsilon\mathcal{M}}{r^2} \left(1 + \frac{P}{\epsilon}\right) \left(1 + \frac{4\pi r^3 P}{\mathcal{M}}\right) \left(1 - \frac{2\mathcal{M}}{r}\right)^{-1}, \quad (3)$$

$$\frac{d\mathcal{M}}{dr} = 4\pi r^2 \epsilon, \quad \frac{d\nu}{dr} = -\frac{2}{P + \epsilon} \frac{dP}{dr}, \quad (4)$$

where  $P$  is the pressure,  $\epsilon$  is the energy density,  $\mathcal{M}$  the gravitational mass at radius  $r$ , and  $\nu(r)$  the temporal metric function in the Schwarzschild-like metric.

**Dynamical equilibrium:** One can go beyond these hydrostatic equations by solving the Gondek's radial oscillation equations [75] which consist of a pair of coupled first-order differential equations for the relative radial displacement  $\Delta r/r \equiv \xi$  and Lagrangian perturbed pressure  $\Delta P$  (implicitly having factors of  $e^{i\omega_n t}$  and  $G = c = 1$ ) written in matrix form as [75]:

$$\begin{pmatrix} \frac{d\Delta P}{dr} \\ \frac{d\xi}{dr} \end{pmatrix} = \begin{pmatrix} \mathcal{Z}(r) & \mathcal{Q}(r, \omega_n^2) \\ \mathcal{R}(r) & \mathcal{S}(r) \end{pmatrix} \begin{pmatrix} \Delta P \\ \xi \end{pmatrix}, \quad (5)$$

where  $\omega_n^2$  is the oscillation eigenvalue and  $\mathcal{Z}, \mathcal{Q}, \mathcal{R}, \mathcal{S}$  are radial functions giving by [75]

$$\mathcal{Z}(r) = -4\pi r e^\lambda (\epsilon + P) + \frac{1}{\epsilon + P} \frac{dP}{dr}, \quad (6)$$

$$\begin{aligned} \mathcal{Q}(r, \omega^2) &= -8\pi r P (\epsilon + P) e^\lambda + \\ &\frac{r}{\epsilon + P} \left(\frac{dP}{dr}\right)^2 - 4\frac{dP}{dr} + \omega^2 r (\epsilon + P) e^{\lambda - \nu}, \end{aligned} \quad (7)$$

BC	$P$	$\mathcal{M}$	$\nu$	$\lambda$	$\xi$	$\Delta P$
$r = 0$	$P_0$	0	$\nu_0$	0	1	$-3(\xi P \Gamma)_{\text{center}}$
$r = R$	0	$M$	$\ln(1 - 2M/R)$	$-\nu(R)$	finite	0

TABLE II. Set of boundary conditions (BC) at the NS center ( $r = 0$ ) and surface ( $r = R$ ) to solve simultaneously the TOV+Gondek's equations, with ' $\nu_0$ ' chosen appropriately.

JC	Rapid	Slow
$\xi(r = r_{\text{inter}})$	$[\xi - \Delta P / (rP')]_{-}^{+} = 0$	$[\xi]_{-}^{+} = 0$
$\Delta P(r = r_{\text{inter}})$	$[\Delta P]_{-}^{+} = 0$	$[\Delta P]_{-}^{+} = 0$

TABLE III. Radial oscillation junction conditions (JC) at the interface ( $r_{\text{inter}}$ ) for rapid and slow conversions. Note that  $[\xi]_{-}^{+} \equiv \xi^{+} - \xi^{-}$  and  $[\Delta P]_{-}^{+} \equiv \Delta P^{+} - \Delta P^{-}$ , meaning  $+(-)$  to the right (left) of the interface with increasing  $r$ . Besides,  $P' \equiv dP/dr$ , where ' $P(r)$ ' is a solution of the TOV equations.

$$\mathcal{R}(r) = -\frac{1}{r} \frac{1}{P\Gamma}, \quad \mathcal{S}(r) = -\frac{1}{\epsilon + P} \frac{dP}{dr} - \frac{3}{r}, \quad (8)$$

being  $\Gamma(r) = (1 + \epsilon/P)c_s^2$  the adiabatic index and  $\lambda(r) = -\ln(1 - 2M/r)$  the spatial metric function of the Schwarzschild-like metric.

**Set of boundary conditions:** In order to solve this system of coupled equations, Eqs. (3)–(8), we list the required boundary conditions in Table II, where the main input is the EoS,  $P = P(\epsilon)$ , characterizing the NS phases.

Nevertheless, 1st-order phase-transition discontinuities in the EoS require further boundary conditions, especially for the radial-oscillation problem due to the existence of two co-existing phases at some given radius [76, 77]. In Table III we list them, where only the extreme cases of slow and rapid junction conditions (JC) are dealt with.

**Reaction modes in twin stars?** It is worth to mention that in the case of rapid JCs, one extra highly non-trivial radial mode appears, the so-called *reaction mode*, which is present only when strong transitions occur at NS interiors [77]. This mode becomes relevant when pass to be the fundamental one with eigenfrequency  $\omega_{n=0}^2 \equiv \omega_R^2$  for delicate combinations of  $P_t$ ,  $\Delta\epsilon$  and  $\eta \equiv \epsilon_{\text{Q}}^{\text{min}}/\epsilon_{\text{H}}^{\text{max}}$ , i.e.  $\omega_R^2 \sim (3[1 + P_t/\epsilon_{\text{H}}^{\text{max}}] - 2\eta)/(\eta - 1)$  [77]. In the next sections, we will verify if this reaction mode really appears or not in twin stars for our employed JCs.

## III. THE QCD TRACE ANOMALY WITH STRONG TRANSITIONS

**Overview:** A few years after asymptotic freedom was discovered within pQCD, it was realized non-perturbatively in Refs. [78, 79] that (even by assuming massless quark flavors), the trace of the energy-momentum tensor of QCD, i.e.  $\eta_{\mu\nu} T_{\text{QCD}}^{\mu\nu}$  (being ' $\eta_{\mu\nu}$ ' the Minkowski metric tensor) possesses a so-called *quantum*

*anomaly* associated to the dynamical breaking of scale-conformal invariance induced purely by the highly non-trivial nature of the real QCD vacuum. If one turns on the quark masses, the aforementioned trace passes to include an explicit breaking directly connected to the quark condensates. These results are given by [78, 79]

$$\eta_{\mu\nu} T_{\text{QCD}}^{\mu\nu} \equiv T_{\mu}^{\mu} = \frac{\beta_{\text{QCD}}}{2g} G_{\mu\nu}^a G_a^{\mu\nu} + (1 + \gamma_m) \sum_f m_f \bar{q}_f q_f, \quad (9)$$

where  $\{G_{\mu,\nu}^a, q_f\}$  are the renormalized gluon and quark fields,  $\{m_f, g\}$  the renormalized quark masses and gauge coupling, ' $\beta_{\text{QCD}}$ ' is the QCD beta function and ' $\gamma_m$ ' is the anomalous dimensions of the quark mass. Notice that Eq. (9) is valid for perturbative as well as non-perturbative energy scales. Besides, the behavior of this anomaly depends upon the number of active flavors. It is interesting to note that as of today, only pQCD results for ' $\beta$ ' and ' $\gamma_m$ ' are reliably known.

**In-medium case:** If one is interested in the equilibrium thermodynamics of Eq. (9), it is appropriate to separate the vacuum and in-medium (dense and thermal) contributions in order to build the thermal average of the non-vacuum sector as

$$\langle T_{\mu}^{\mu} \rangle_{\mu_B, T} = \epsilon - 3P \quad (10)$$

According to Ref. [33], one can work more appropriately with its normalized version given by<sup>4</sup>

$$\Delta \equiv \frac{\langle T_{\mu}^{\mu} \rangle_{\mu_B, T}}{3\epsilon} = \frac{1}{3} - \frac{P}{\epsilon}. \quad (11)$$

Interestingly, it was proven in Ref. [33] that this quantity has the extreme values between ( $T = 0$  and  $\mu_B \neq 0$ )

$$-\frac{2}{3} (\approx -0.667) \leq \Delta < \frac{1}{3} (\approx 0.333), \quad (12)$$

the lower bound coming from the non-relativistic limit ( $P \ll \epsilon$ ) and the upper bound from the causality bound ( $P \leq \epsilon$ ), while the conformal (ultra-relativistic) limit lies at  $\Delta = 0$ . This allows us to write  $c_s^2$  as  $c_s^2(\Delta)$ , i.e.

$$c_s^2 = c_{s, \text{deriv}}^2 + c_{s, \text{nonderiv}}^2, \quad (13)$$

where these new terms (derivative and non-derivative) are defined as follows [33]:

$$c_{s, \text{deriv}}^2 \equiv -\epsilon \frac{d\Delta}{d\epsilon}, \quad c_{s, \text{nonderiv}}^2 \equiv \frac{1}{3} - \Delta, \quad (14)$$

being the conformality of the system reached when  $\Delta \rightarrow 0$  and  $d\Delta/d\epsilon \rightarrow 0$ , i.e.  $c_s^2 \simeq c_{s, \text{nonderiv}}^2 \rightarrow 1/3$ .

<sup>4</sup> With this definition, one can see explicitly its scale-invariant nature, i.e. defining the dimensionless  $P' = P/\epsilon^*$  and  $\epsilon' = \epsilon/\epsilon^*$ , one gets an adimensional quantity  $\Delta = 1/3 - (P'\epsilon^*)/(\epsilon'\epsilon^*) = \Delta' = 1/3 - P'/\epsilon'$ , being  $\epsilon^*$  some appropriate energy-density scale.

**Behavior of ' $\Delta$ ' in the mixed phase:** Now, for our investigation of  $\Delta$  in the interior of NSs with first-order phase transitions, we solve Eq. (14) with our hadronic and QM EoSs after finding  $c_s^2$  for each phase. Apart from the numerically straightforward result  $\Delta_H$  from  $c_{s,H}^2$  for the hadronic phase, the mixed phase satisfies  $c_s^2 = 0$  (since  $P_t$  is constant within the Maxwell construction), with Eq. (14) becoming the following differential equation and respective initial condition being the maximal hadronic energy density before the transition:

$$\epsilon \frac{d\Delta_{\text{mix}}}{d\epsilon} + \Delta_{\text{mix}} = \frac{1}{3}, \quad \Delta_{\text{mix}}(\epsilon_H^{\text{max}}) \equiv \Delta_H^{\text{max}}, \quad (15)$$

with general solution given by

$$\Delta_{\text{mix}}(\epsilon) = \frac{1}{3} \left( 1 - \frac{\epsilon_H^{\text{max}}}{\epsilon} \right) + \frac{\epsilon_H^{\text{max}}}{\epsilon} \Delta_H^{\text{max}}, \quad (16)$$

which in turn leads us to obtain  $c_{s, \text{deriv}, \text{mix}}^2$  as

$$c_{s, \text{deriv}, \text{mix}}^2 = \frac{\epsilon_H^{\text{max}}}{\epsilon} \left( \Delta_H^{\text{max}} - \frac{1}{3} \right) = -c_{s, \text{nonderiv}, \text{mix}}^2. \quad (17)$$

One should be careful with the interpretation of Eqs. (16)–(17). Firstly,  $\Delta_{\text{mix}}(\epsilon)$  cannot be considered physical within our Maxwell construction, but it should be understood as an artifact that joins  $\Delta_H$  to  $\Delta_Q$  in a  $\Delta$  vs  $\epsilon$  plane. Besides, it will be clear from our figures below that in all cases that  $\Delta_{\text{mix}}$  is an smooth increasing curve (strickly speaking, a branch of a negative rectangular hyperbolae) although we do not display their explicit behavior keeping that region in blank. In few words, the  $\Delta\epsilon$  jump induces a smooth jump in  $\Delta(\epsilon)$ . Interestingly, this behavior was also found in Ref. [67] within their deep neural network calculations but without physical explanation. Secondly, Eq. (17) explains the opposite nature of these terms at the mixed phase which for us is unphysical, but it can be highly non-trivial if one allows the formation of (electrically-charged) crystalline structures with the Gibbs/Glendenning constructions [12].

**Onset to the QM phase:** After the strong transition occurs, the  $\Delta_Q$  for the QM phase (with  $c_s^2 = \text{const} \equiv s$  within our CSS parametrization) from Eq. (14) produces

$$\epsilon \frac{d\Delta_Q}{d\epsilon} + \Delta_Q = \frac{1}{3} - s, \quad \Delta_Q(\epsilon_Q^{\text{min}}) \equiv \Delta_Q^{\text{min}}, \quad (18)$$

the last term being the initial boundary condition at the minimal value of QM energy density after the transition having the following general solution

$$\Delta_Q(\epsilon) = \left( \frac{1}{3} - s \right) \left( 1 - \frac{\epsilon_Q^{\text{min}}}{\epsilon} \right) + \frac{\epsilon_Q^{\text{min}}}{\epsilon} \Delta_Q^{\text{min}}, \quad (19)$$

which leads to

$$c_{s, \text{deriv}, Q}^2 = \frac{\epsilon_Q^{\text{min}}}{\epsilon} \left( \Delta_Q^{\text{min}} + s - \frac{1}{3} \right) = s - c_{s, \text{nonderiv}, Q}^2. \quad (20)$$

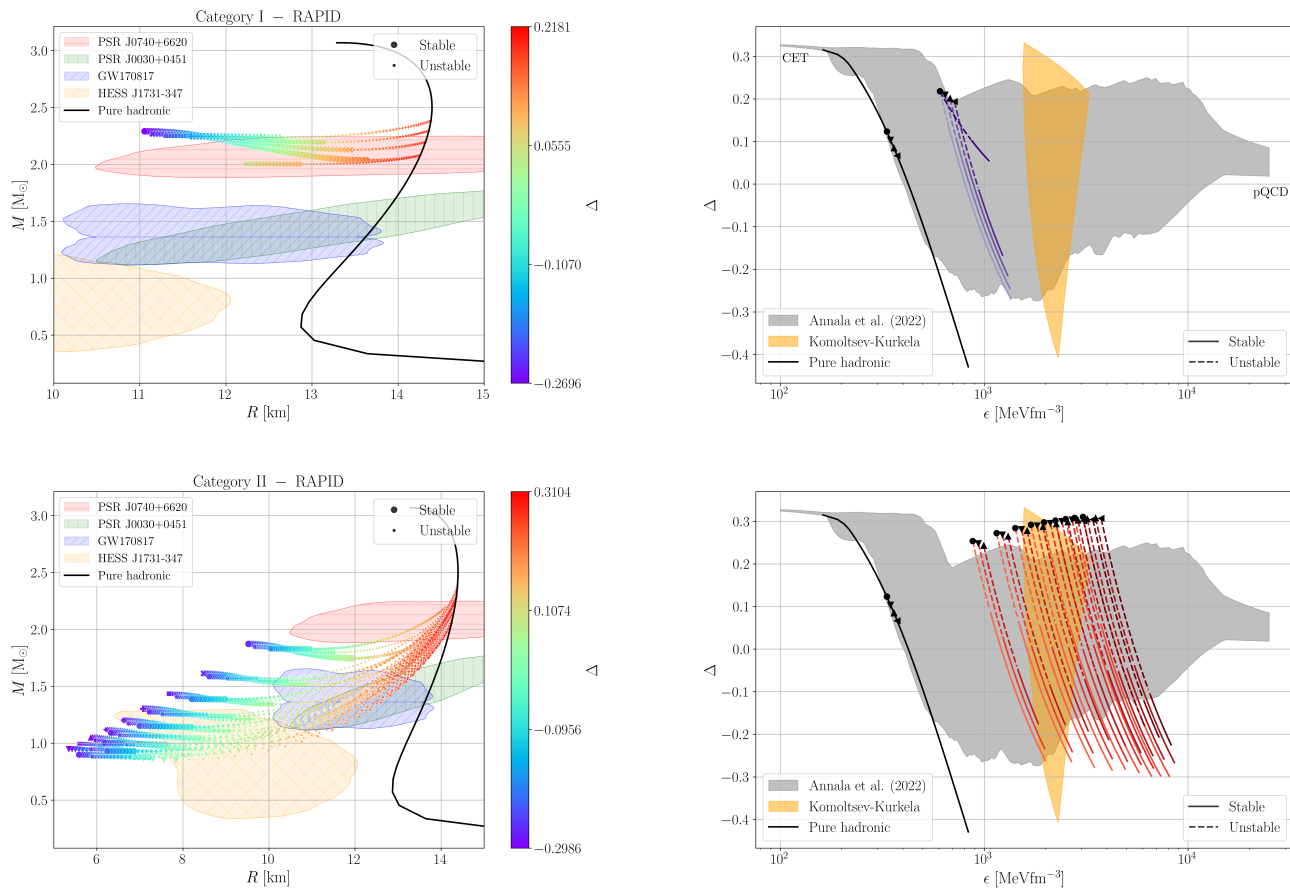


FIG. 3. *Left panels*:  $M$ – $R$  relations for twin stars belonging to Categories I (upper panel) and II (lower panel) (including various current astrophysics constraints) with a range of colours on the right side indicating values for their corresponding trace anomalies. Note that thick (thin) colored and filled circles indicate stable (unstable) twins in the sense of radial pulsations. *Right panels*: Dense trace anomaly as a function of energy density,  $\Delta = \Delta(\epsilon)$ , where we include constraints coming from CET (continuous black curve), Komoltsev-Kurkela [74] (orange band), Annala et al. [20] (grey band) and pQCD [22]. Besides, the black dots and differently-oriented triangles represent the jumps in Eq. (16) which one has to read from left to right, e.g. a given left (low energy densities) triangle starts to obey Eq. (16) until the same triangle appears on the right (higher energy densities), where the QM phase begins. Note that (dis)continuous colored QM curves indicate (un)stable twin stars.

Now, Eqs. (19)–(20) are physical and one can extract qualitative information, which will be explicitly given in the next section. In particular, Equation (19) for  $\Delta_Q$  show us that if  $s > 1/3$ , then it will be a steep decreasing function easily approaching negative values in the ultra-dense sector of twin stars. We will see later that this behavior is also manifested in the  $\Delta_Q = \Delta_Q(\mu_B)$  plane. On the other hand, Eq. (20) tell us that the derivative and nonderivative terms are complementary if  $s$  is large ( $\sim 1$ ), i.e. increasing  $c_{s,\text{nonderiv},Q}^2$  implies decreasing  $c_{s,\text{deriv},Q}^2$  meaning that the high-negative slope of  $\Delta(\epsilon)$  is favored for large  $s$  and at increasing energy densities.

#### IV. TWIN-STAR TRACE ANOMALIES

We pass to employ and solve all the twin EoSs, TOVs, radial oscillation equation with rapid (Sec. IVA) and slow (Sec. IVB) junction conditions to obtain the whole be-

havior of  $\Delta$  for the chosen parameters of Secs. II and III. It is worth to mention again that from all the available parameter space satisfying Eq. (1) giving thousands of twin stars, we only display our findings for tens of EoSs (of all categories) for clear analysis and space limitations.

For comparison with all our figures of this section and Appendix D, in the left panel, we show the current observational constraints from PSR J0740+6620 [16], PSR J0030+0451 [16], GW170817 (spectral EOS) [80] and HESS J1731-347 [81]. In order to not clutter the figure, we have preferred to show only the NICER data from Ref. [16] (not from Ref. [17]). Also, the LIGO data from GW170817 [80] is shown from the spectral EOS analysis (not from universal relations). For the right panels, we put the grey and orange bands of Annala et al. [20] and Komoltsev-Kurkela [74], respectively, of Sec. IIA. These last comparisons serve as a guide but not to agree with since those works did not explore this twin-star topics.

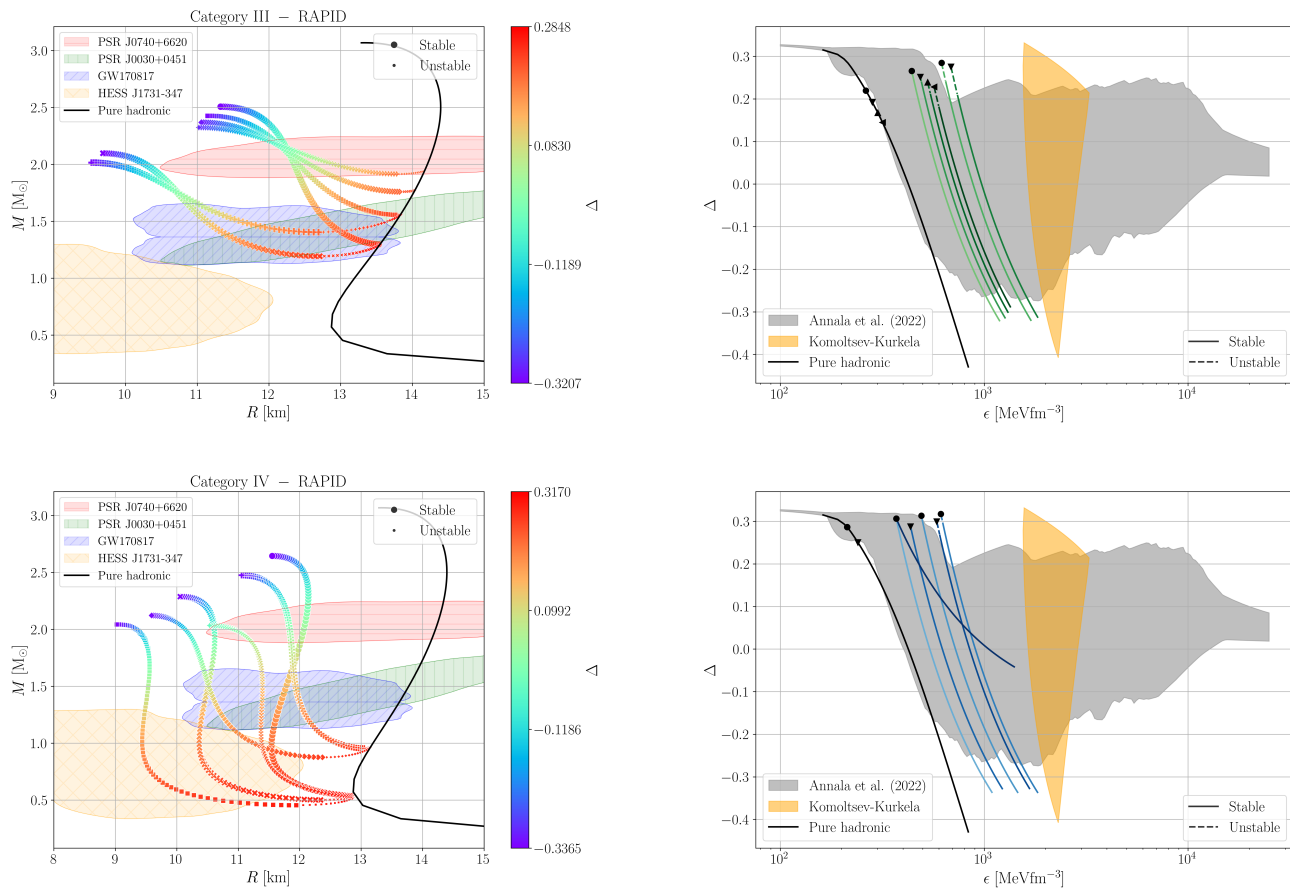


FIG. 4. Same captions and constraints as Fig. 3 but now for twin stars from Categories III and IV.

### A. Rapid conversions

**Categories I and II:** In the left panels of Fig. 3, we present the  $M$ - $R$  relations for twin stars of Categories I and II. One can see that twin stars from those categories satisfy almost all the aforementioned current  $M$ - $R$  constraints except Category I that marginally respects GW170817 and disagrees with HESS J1731-347.

Now, in the right panels of Fig. 3, we display the corresponding behavior of the twin-star trace anomalies as a function of their energy densities for the same two categories. One can easily see that most configurations present not only  $\Delta < 0$  for a wide range of densities in the QM phase, but they also decrease abruptly, reaching quickly negative values for ultra-dense stable twins (continuous curves). It is also worth to mention that Category I twins does not approach pQCD since they do not pass through the Komoltsev-Kurkela orange band. This is in contrast to the behavior of  $\Delta$  for Category II twins although only the unstable twins pass through this orange band while the stable stars accumulate at higher densities (see discussion in Sec. IIA about the Komoltsev-Kurkela region).

Besides, for all twin configurations of Category I with  $c_{s,Q}^2 = 1$  in the QM phase, we have a negative  $\Delta$  in the

high density regime. Only when  $c_{s,Q}^2 = 0.5$ , we were able to find stable twins, but  $\Delta$  remaining positive for all densities ( $M$ - $R$  relation with the smallest hybrid masses and  $\Delta = \Delta(\epsilon)$  with different slope, both displayed in the upper panels in Fig. 3). Besides, unlike Category I, Category II twin stars were only stable for  $c_{s,Q}^2 = 1$ , leading stringently to negative trace anomalies for high densities. In this sense, considering a high enough central density, stable Category II twin stars always presented a negative trace anomaly in their cores.

**Categories III and IV:** For these categories shown in Fig. 4, we found similar scenarios than the left panels of Fig. 3 for the  $M$ - $R$  relations being or not in agreement with astrophysics constraints, in particular, Category I is similar to III and Category IV is similar to II, but of course, each one with its own differences between categories. On the other hand, on the right panels of Fig. 4, one can identify that the trace anomaly is always negative for these twin-stars configurations surpassing the  $2M_{\odot}$  limit, i.e. massive twin stars. The reader can also see that all of them are dynamically stable against radial pulsations if and only if  $c_{s,Q}^2 = 1$ .

However, if for the particular case of Category IV twins one instead employs  $c_{s,Q}^2 = 0.5$  for the QM phase in the CSS parametrization, we found a single stable configura-



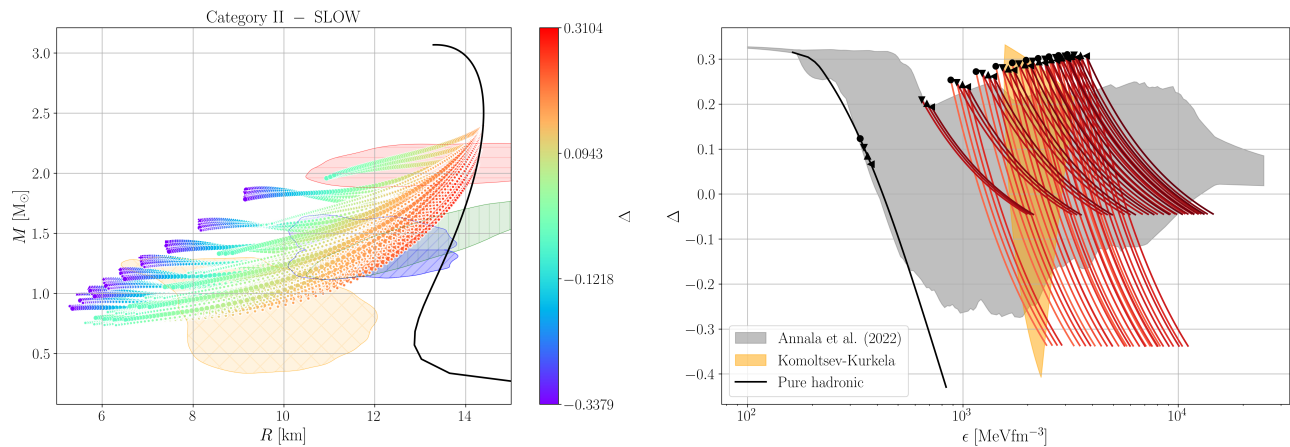


FIG. 5. Same captions and constraints as in Fig. 3 but from Category II twin considering now slow junction conditions.

tion. In other words, the stability and robustness of the negative values of  $\Delta$  in twin-star matter depends strongly on the high values we employ for the (squared) speed of sound for the QM phase, i.e.  $0.5 \leq c_{s,Q}^2 \leq 1$ . Finally, the reader can realize that the orange regions of Komoltsev-Kurkela (in the right panels), is not reached by the twin stars of these categories. Of course, and as already discussed in Sec. IIA, this band should serve to make not too strict comparisons since their conclusions assumed potential hybrid NSs with ultra-dense phase not reaching such high densities, i.e. above  $n_B = 10n_0$ .

#### Twin-star stability through the reaction modes:

In order to close our discussion on these rapid-conversion twin stars, we pass to give particular comments connected to the so-called *radial reaction modes* [77]. As shown in Ref. [77], when one considers rapid junction conditions at the strong-transition point of hybrid stars, it will inevitably lead to the appearance of a reaction mode which, in principle, may be any excited ( $n \geq 0$ ) radial mode but becomes of importance when it is the fundamental one ( $n = 0$ ). From our calculations with rapid twin stars, we found that the fundamental mode is always the reaction mode since  $\Delta\epsilon$  is a relatively large value, something which is not necessarily true for connected hybrid stars, as already explored in Ref. [77]. This also highlights the different stability windows for rapid and slow twin stars, since for the rapid ones the hadronic and hybrid branches are disconnected because unstable configurations emerge, but nonviable for slow twins.

### B. Slow conversions

Next, we move to describe the results of our calculations for twin star configurations but now employing the *slow* junction conditions in the radial pulsation equations, as formulated in Table III. Being more specific, the main feature of these stars in the  $M$ - $R$  diagram is that the hybrid branch becomes connected to the hadronic one, i.e. both branches remain stable without interme-

diating unstable stars. Besides, it is worthy of note that the usual stability criterion ( $\partial M/\partial\epsilon_c \geq 0$ ) does not correspond with the sign of the fundamental frequency in this case [77], therefore, other EoSs become valid (not presented in Fig. 2 for clarity and space limitations).

In particular, we have many more viable EoSs corresponding to Category II twin stars that only have a stable hybrid branch in the slow scenario. The results for other categories do not change significantly and may present slightly larger stability windows within the parameter space agreeing with the Seidov's criterium, i. e. the last stable configuration occurs for larger central densities when compared to the rapid case. For the aforementioned reasons, we only show in Fig. 5 the results for Category II twin stars.

In the left panel, we present the  $M$ - $R$  relations, while in the right panel its corresponding trace anomalies as functions of energy density. One can see that many configurations that were unstable in the rapid case are now stable in the slow case (see e.g. Ref. [70] for a similar discussion). In fact, the HESS J1731-347 [81] can be seen as slow-stable hybrid star [82].

Notice also that in the right panel of Fig. 5 the curves for the stability paths of the ultradense twins pass mostly over the Komoltsev-Kurkela orange band although with different slopes, i.e. the darker curves having lower slopes than the lighter ones. It is worth to mention that these darker curves with less negative slope correspond to  $c_s^2 = 0.5$ , and they are present in a significantly larger number of stable configurations when compared to the rapid scenario. In particular, we found only two stable configurations in the rapid case for  $c_s^2 = 0.5$ , for Categories I and IV, with the former presenting an always positive trace anomaly, which does not happen in the slow scenario, where it is clear that  $\Delta < 0$  for higher densities. Nevertheless, there still remain some high-density configurations which accumulate slightly below the pQCD limit at  $n_B = 40n_0$  (see related discussion at Sec. IIA).

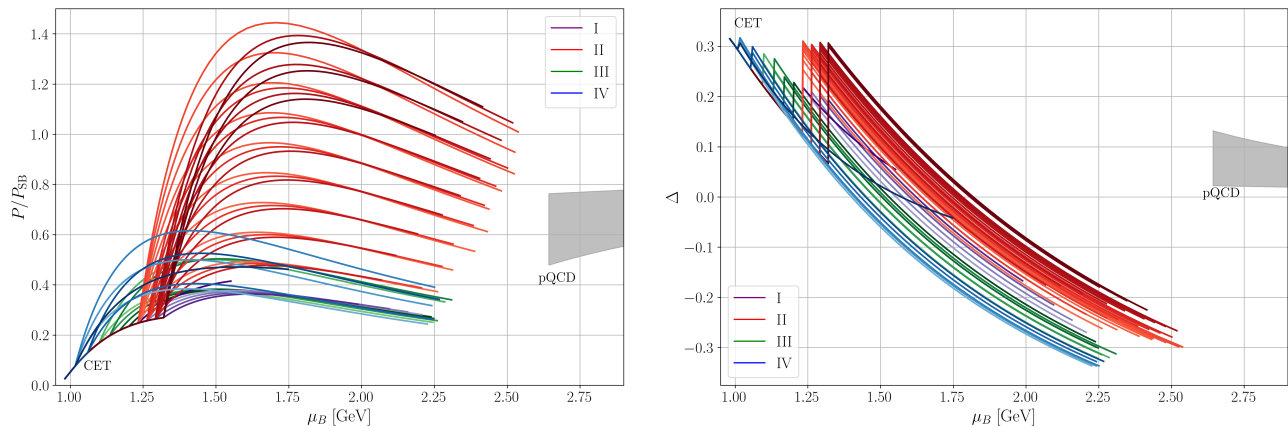


FIG. 6. *Left panel:* Behavior of our *rapid* twin-star normalized (by a Stefan-Boltzmann gas) pressures for each category vs baryon chemical potential. Notice the presence of the hadronic CET and quark pQCD bands, this last one appearing at  $\mu_B = 2.6$  GeV corresponding to  $n_B = 40n_0$ , as in other works (see e.g. Ref. [20]). *Right panel:* Dense trace anomalies vs baryochemical potential for the four categories of twin stars. The pQCD band ( $\mu_B \geq 2.6$  GeV) is thicker than the CET one.

## V. DISCUSSION

From our above results for the discontinuous and negative twin-star trace anomalies, an immediate question would be to know the fundamental behavior of  $\Delta$ , i.e.  $\Delta = \Delta(\mu_B)$ , since that way it could be obtained from the thermodynamic Landau potential of QCD,  $\Omega(\mu_B) = -P(\mu_B)$ , as occurs with LQCD at pure  $T \neq 0$  [5, 6]. Interestingly, futuristic baryonic results from LQCD (or other novel non - perturbative QCD techniques) could reliably characterize this quantity at  $\mu_B \neq 0$  and determine if it is truly negative/discontinuous around a 1st-order transition point, today still being an open question.

For these reasons, it becomes relevant first to understand the behavior of  $P = P(\mu_B)$ , or more precisely, its normalized form,  $P/P_{\text{SB}}$ , being  $P_{\text{SB}} = (3/4\pi^2)(\mu_B/3)^4$  the Stefan-Boltzmann pressure. In fact, within the CSS parametrization, it was proven in Ref. [72] that the QM pressure could be written as

$$P_Q(\mu_B) = N\mu_B^{1+\gamma} - B, \quad (21)$$

with the constant parameters listed in Table IV for a family of twin stars within each category. Besides, if this  $P_Q$  is normalized by  $P_{\text{SB}}$ , one easily verify that it becomes increasing from the transition point, reaches a maximum, and then begins to decrease.

In Fig. 6, we display (for the first time in the literature of twin stars with the CSS parametrization) these outcomes for the same twin-star EoSs from the left panel of Fig. 2 for our four categories after imposing the rapid junction conditions in the radial pulsation problem. One can see that Category III and IV twin stars do not change too abruptly their normalized pressure at the transition point, then reaching maximal values of  $P/P_{\text{SB}} \sim 0.4 \pm 0.2$ , where it seems difficult for those pressures to reach the pQCD (grey) band at  $\mu_B = 2.6$  GeV. On the other hand,

Category I and II twin stars present strong discontinuities in this  $P/P_{\text{SB}} - \mu_B$  plane, but equally interesting are the maximal values they reach, i.e.  $P/P_{\text{SB}} \sim 1 \pm 0.4$ , and showing a favored trend towards pQCD if extrapolated to higher densities.

Some comments about the relation of these last findings compared to current studies of the NS EoS are in order. In particular, Bayesian approaches (see, e.g. [52, 83, 84]) and other works having microphysics control (see, e.g. Ref. [45]) sometimes build their predictions for the EoS at intermediate densities not only through relations like  $P = P(\epsilon)$ , but also in the plane  $P/P_{\text{SB}}$  vs  $\mu_B$ . Remarkably, most of these works always assume bands of uncertainty satisfying  $P/P_{\text{SB}} \leq 1$ , even considering the potential presence of phase transitions, in order to reach pQCD at high densities by increasing the values of  $P/P_{\text{SB}}$ , in other words, from below the pQCD band. However, our results of the left panel of Fig. 6 for Category I and II twin stars indicates that it could still possible to reach pQCD with a decreasing  $P/P_{\text{SB}}$ , i.e. from above as large as  $[P/P_{\text{SB}}]_{\text{max}} \sim 1.4$ . Thus, this novel and intriguing possibility could further constrain the NS EoS.

Furthermore, a few years ago, Ref. [33] pointed out that  $\Delta \geq 0$  in NS interiors due to the increasing number of effective degrees of freedom,  $N_{\text{eff}}$ , i.e.  $\Delta \sim d(P/P_{\text{SB}})/d\mu_B \sim dN_{\text{eff}}/d\mu_B$  being always positive definite. Our viewpoints about  $\Delta(\mu_B)$  with strong transition are the following: these discontinuous transitions are tightly connected to a finite value of the latent heat,  $Q$ , through

$$Q = \mu_c \Delta n_B = [T_\mu^\mu(\mu_B^+ \rightarrow \mu_c)]_Q - [T_\mu^\mu(\mu_B^- \rightarrow \mu_c)]_H, \quad (22)$$

where the symbols  $\mu_B^{+(-)} \rightarrow \mu_c$  mean ‘approach from the left (right) to the critical baryochemical potential’. From Table IV it is straight to infer that these  $Q$ ’s are non -

Category	$Q$	$\gamma = 1/c_{s,Q}^2$	$\epsilon_0$	$N$	$B$
I	274.26	1.0	811.59	$3.13 \times 10^{-4}$	405.80
II	545.80	1.0	1354.68	$4.91 \times 10^{-4}$	677.34
III	178.38	1.0	590.00	$2.69 \times 10^{-4}$	295.00
IV	157.94	1.0	518.76	$2.60 \times 10^{-4}$	259.38

TABLE IV. The latent heat from Eq. (22) for each twin-stars category, alongside the parameters required to obtain the baryon chemical potential and baryon density in the CSS parametrization [72]. Note that  $Q, \epsilon_0 = (1 + \gamma)B$  and  $B$  are in  $\text{MeV fm}^{-3}$ , while ‘ $N$ ’ is in  $\text{MeV}^{-\beta} \text{fm}^{-3}$  and ‘ $\gamma$ ’ is in units of the inverse of the speed of light squared, i.e. dimensionless.

negligible in these four twin-star categories. Equivalently, one can write this ‘ $Q$ ’ in a normalized form as

$$\frac{Q}{\mu_c^4} = \mu_c \left[ \left( \frac{dN_{\text{eff}}^Q}{d\mu_B^+} \right) - \left( \frac{dN_{\text{eff}}^H}{d\mu_B^-} \right) \right]_{\mu_B^\pm \rightarrow \mu_c}, \quad (23)$$

where  $N_{\text{eff}}^Q \equiv P_Q/\mu_B^4$  and  $N_{\text{eff}}^H \equiv P_H/\mu_B^4$  are the effective degrees of freedom at each quark (Q) and hadronic (H) phases. In other words, first-order transitions modify abruptly the degrees of freedom in the system through a discontinuous behavior of the trace anomaly leading (as we have proven above in the energy-density plane and below vs baryon chemical potential) to non-negligible negative values. This delicate and non-trivial observation can be considered an extension of the general study of Ref. [33]. Related to this, Ref. [68] explored (slightly) weak 1st-order transitions in NSs having  $Q \sim 0$ , since at  $\epsilon \sim 700 \text{ MeV fm}^{-3}$ , one has  $N_{\text{eff}}^H \sim N_{\text{eff}}^Q = \text{constant}$ , which for them implies a saturation of degrees of freedom, thus offering a little (negligible) effect on  $\Delta$  to be noticed.

The corresponding  $\Delta(\mu_B)$  for twin star matter at all densities can be written as follows:

$$\Delta(\mu_B) = \begin{cases} \Delta_H(\mu_B) & \mu_B < \mu_c, \\ \Delta_Q(\mu_B) & \mu_B > \mu_c \end{cases} \quad (24)$$

where at  $\mu_B = \mu_c$  suffers a discontinuous jump. This can be clearly seen in the right panel of Fig. 6, where at intermediate ‘ $\mu_B$ ’ the four categories decrease until ‘ $\mu_c$ ’ (vertical lines), from which it increases to then decrease discontinuous (and somewhat steeply) in the QM phase to reach sizeable negative values. Furthermore, the latent heats,  $Q$ , for Category I and II twin stars are larger compared to Categories III and IV, thus signaling a substantial change of effective degrees of freedom, according to Eq. (23). Noteworthy, the normalized quark trace anomaly can be explicitly written from Eq. (21) as

$$\Delta_Q = \frac{4B - 3N\gamma\mu_B^{1+\gamma} (c_{s,Q}^2 - 1/3)}{B + N\gamma\mu_B^{1+\gamma}}, \quad (25)$$

being positive (negative) if  $c_{s,Q}^2 < 1/3 (> 1/3)$ , and of course, assuming reasonable values for ‘ $B$ ’ and ‘ $N$ ’, as those listed in Table IV.

## A. Why ‘ $\Delta < 0$ ’ at twin-star cores?

As somewhat discussed in previous sections, only non-perturbative QCD calculations of  $\Delta(\mu_B)$ , will fully explain its discontinuous negativity (or not) around the transition point. However, while waiting for those results, we can still provide some estimates which exhibit the main features of our numerical findings and taking advantage of their analytic forms within some simplified models for hadronic and quark matter (building twin-star EoSs as a whole) and probe if  $\Delta < 0$  can emerge naturally and robustly or as an artificial phenomena depending only on the specific values chosen for the free parameters. To do this, we elaborate models for each phase, then pointing out situations leading to  $\Delta_{H,Q} < 0$ .

**Hadronic model:** As in Ref. [33], we choose a model inspired by mean-field quantum hadrodynamics with

$$P_H = \left( \frac{C^*}{\Lambda^2} \right) n_B^2 = \left( \frac{\Lambda^2}{4C^*} \right) (\mu_B - m_N)^2, \quad (26)$$

where  $m_N = N_c \Lambda_{\text{QCD}}$  is the baryon mass ( $N_c$  are the number of colors and  $\Lambda_{\text{QCD}}$  the non-perturbative QCD scale),  $C^*$  is the typical interaction strength, and  $\Lambda$  the scale of the system. Within this model, one has that the non-normalized trace anomaly is

$$[T_\mu^\mu]_H = m_N n_B - 2 \left( \frac{C^*}{\Lambda^2} \right) n_B^2, \quad (27)$$

which, in principle, is allowed to be negative if there is some critical baryon density  $n_B^*$  from which

$$n_B > \frac{m_N \Lambda^2}{2C^*} (\equiv n_B^*) \text{ or } n_B = a n_B^*, \text{ with } a > 1, \quad (28)$$

being ‘ $a$ ’ an arbitrary number. Interestingly, from this one can directly obtain a simple expression for the (negative) normalized trace anomaly when

$$\Delta_H = \frac{2}{3} \left( \frac{1-a}{a+2} \right) < 0 \text{ if } a > 1. \quad (29)$$

This implies its (squared) speed of sound to be

$$c_{s,H}^2 = \frac{2C^*}{\Lambda^2} \left( \frac{n_B}{m_N + 2(C^*/\Lambda^2)n_B} \right) = \frac{a}{1+a}, \quad (30)$$

which means that for the lowest (highest) values satisfying this condition, one has, e.g.,  $a = 1.01$  (1000) giving  $c_{s,H}^2 \simeq 0.5$  (1), respectively. This leads us to infer that any hadronic model will have  $\Delta_H < 0$  for large speeds of sound (in fact, this was already found in Ref. [85] for the well-known hadronic APR and TM1 EoSs having large  $c_s^2$  at intermediate densities). In Appendix B we prove that this feature of  $\Delta_H < 0$  is robust enough even if we exchange quantum hadrodynamics model by a polytrope. Besides, in the right panels of Figs. 3–4 and 5 we present results of  $\Delta$  for our CET model (*pure hadronic*, black curves), where one can easily see their negative behavior.

**Quark model:** Inspired by Ref. [72] for its CSS EoS and corresponding Eq. (21) for  $P_Q(\mu_B)$ , we propose the more generic pressure including a condensation term which could potentially lead to the same CSS EoS. This is motivated by the fact that at cold and finite isospin densities, LQCD calculations [11] and effective models [86] have concluded that the main reason for their  $\Delta$  be negative is the dominating condensation term at intermediate densities. We will test its importance in this CSS model for intermediate  $\mu_B$  at the neighborhood of the transition point. Then, our proposed pressure is<sup>5</sup>

$$P_Q \equiv N\mu_B^{1+\gamma} + C\mu_B^{(1+\gamma)/2} - B, \quad (31)$$

where ‘ $N$ ’ and ‘ $C$ ’ are related to ‘ $N_{\text{eff}}$ ’ and a non-perturbative *condensation* term, respectively. In general, they are running quantities of  $\mu_B$ , i.e.  $N = N(\mu_B)$  and  $C = C(\mu_B)$ . Besides, according to this parametrization [72],  $\gamma \equiv 1/c_{s,Q}^2 = \text{constant}$  and ‘ $B$ ’ would be confinement constant. Of course, in the conformal limit of  $c_{s,Q}^2 = 1/3$ , one has  $\gamma = 3$  for which the factor multiplying ‘ $C$ ’ has a power ‘ $(1 + \gamma)/2$ ’ in order to reproduce known color-flavor locked (CFL) superconductivity results giving  $P_{\text{CFL}} \sim \mu_B^2$ , which in total gives the widespread [77, 87, 88] pressure  $\sim a_4\mu_B^4 + a_2\mu_B^2 - B$ , being  $a_2, a_4$  some phenomenological constants.

As expected, one can also deduce from Eq. (31) the associated trace anomaly

$$\begin{aligned} [T_\mu^\mu]_Q &= \left[ N(\gamma - 3) + \frac{\partial N}{\partial \ln \mu_B} \right] \mu_B^{1+\gamma} \\ &+ \left[ \left( \frac{\gamma - 7}{2} \right) C + \frac{\partial C}{\partial \ln \mu_B} \right] \mu_B^{(1+\gamma)/2} + 4B, \quad (32) \end{aligned}$$

where we considered the general case of running ‘ $N$ ’ and ‘ $C$ ’. From Eq. (32), one realizes that  $[T_\mu^\mu]_Q$  can be positive or negative, depending mainly on ‘ $\gamma$ ’. For instance, when  $\gamma = 3$  ( $c_{s,Q}^2 = 1/3$ ) and  $\{N, C\} = \text{constants}$ , one gets  $[T_\mu^\mu]_{\text{eMIT}} = 4B - (2C)\mu_B^2$  with  $C = [3/(2\pi^2)] a_2$  for the effective MIT bag model (eMIT) [89], being ‘ $a_2$ ’ the decisive parameter for positiveness or negativeness.

Nevertheless, we need to verify if the presence of the ‘ $C$ ’ term is consistent or not with our CSS parametrization with  $c_{s,Q}^2 = 1/\gamma = \text{constant}$ , i.e. being density independent, since past realistic works (e.g. the eMIT or pQCD) consider density-dependent speeds of sound.

After some manipulations (see Appendix E), the corresponding quark EoS,  $P_Q = P_Q(\epsilon)$ , becomes<sup>6</sup> (assuming

$N = \text{constant}$  implying a fixed number of degrees of freedom in the quark phase)

$$\begin{aligned} P_Q &= \frac{\epsilon}{\gamma} - \left( \frac{\gamma + 1}{\gamma} \right) B + \frac{C_r^2}{8N} \left( \frac{1 - \gamma^2}{\gamma^2} \right) \\ &\pm \frac{C_r}{8N} \left( \frac{\gamma + 1}{\gamma} \right) \sqrt{\left( \frac{\gamma - 1}{\gamma} \right)^2 C_r^2 + \frac{16N}{\gamma} (\epsilon - B)}, \quad (33) \end{aligned}$$

where ‘ $C_r$ ’ is defined in Appendix E. The associated (squared) speed of sound is (still with  $N = \text{constant}$ )

$$\begin{aligned} c_{s,Q}^2 &= \frac{dP}{d\epsilon} = \frac{1}{\gamma} \\ &+ \frac{C_r}{4N} \left( \frac{1 - \gamma^2}{\gamma^2} \right) \left( \frac{dC_r}{d\epsilon} \right) \pm \left( \frac{\gamma + 1}{\gamma} \right) \frac{1}{8N} \sqrt{(\dots)} \left( \frac{dC_r}{d\epsilon} \right) \\ &\pm \left( \frac{\gamma + 1}{\gamma} \right) \frac{1}{\sqrt{(\dots)}} \left[ \frac{C_r^2}{4N} \left( \frac{\gamma - 1}{\gamma} \right)^2 \left( \frac{dC_r}{d\epsilon} \right) + \frac{2C_r}{\gamma} \right], \quad (34) \end{aligned}$$

where ‘ $\sqrt{(\dots)}$ ’ means the square root in Eq. (33). Interestingly, this Eq. (34) indicates that constant ‘ $C$ ’ (leading to  $C_r = C$ ) or running ‘ $C$ ’ (leading to  $C_r \neq C$ ) should not be allowed in the EoS to keep our original assumption of  $c_{s,Q}^2 = 1/\gamma$ . Thus, at  $\mu_B \neq 0$  (in marked contrast to finite isospin densities), one must put  $C \equiv 0$  if we give the speed of sound a constant value in a given range of baryon densities.

With this in mind, Eq. (32) is reduced to (with  $C = 0$  and  $N = \text{constant}$ )

$$[T_\mu^\mu]_Q = N(\gamma - 3)\mu_B^{1+\gamma} + 4B. \quad (35)$$

It might be negative if  $\gamma < 3$ , or equivalently,  $c_{s,Q}^2 > 1/3$ . In this sense, the negativeness of  $\Delta$  comes directly from large  $c_{s,Q}^2$  and not a condensation term (as in isospin matter) which spoils the consistency of the CSS parametrization. Of course, other quark models having control on the degrees of freedom and interactions can clarify this point.

## B. Insights for non-perturbative QCD physics

Last year, in Ref. [52], it was postulated a new parameter  $d_c \equiv \sqrt{\Delta^2 + (\Delta')^2}$  (being  $\Delta' = d\Delta/d \ln \epsilon$ ) as a quantitative (and non-perturbative) measure of *conformality* in strongly interacting matter. In particular, for first-order phase transitions, they found [52]  $\Delta' = 1/3 - \Delta$ . Besides, they established that near conformal (deconfined) matter appear when  $d_c < 0.2$ , thus preventing first-order transitions from masquerading as conformalized matter (see Ref. [52] for details).

For our four (*rapid*) twin-star categories, we show in Fig. 7 the results of our calculations. Compared to Fig. 1 of Ref. [52], one can extract several new features. First of all, the magnitudes for ‘ $d_c$ ’, i.e. now reaching even values

<sup>5</sup> Electrons have a small contribution, which we neglect for sake of simplicity. Besides, do not confuse our constant ‘ $\gamma$ ’ with  $\gamma = d \ln P / d \ln \epsilon$  usually found in the literature, e.g. as in Ref. [52].

<sup>6</sup> We verified that this pressure reproduces the widespread EoSs of Refs. [77, 87, 88]. However, Ref. [87] does not justify the choice of positive sign, whereas Refs. [77, 88] selects correctly the negative sign, although without explicit explanation.

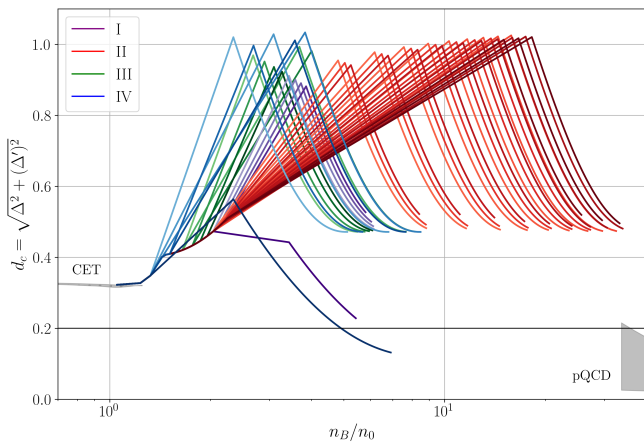


FIG. 7. Quantitative measures of conformality through  $d_c = \sqrt{\Delta^2 + (\Delta')^2}$  [52] as a function of the normalized baryon density,  $n_B/n_0$ . Notice that we keep the colors for each twin-star category as in previous figures. Besides, we draw the horizontal conformality transition at  $d_c = 0.2$ . Again, the CET (thin) and pQCD (thick) grey bands are also showed.

of around 1 due to the jumps in  $\Delta n_b$ . This ‘high’ values were considered impossible in their computations which maximally reached  $d_c \sim 0.6$  taking into account also phase transitions but smoothly, i.e. as rapid crossover. Secondly, our results at the critical point tend to decrease somewhat quickly never go below the conformal transition point of  $d_c = 0.2$ , thus potentially considered as non - conformal (except with a pair of cases from categories I and IV). Thirdly, unlike in Ref. [52], our  $d_c$ ’s could approach the conformal pQCD regime from above, i.e.  $d_c > 0.2$ , thus excluding any possible existence of conformal matter at intermediate densities even having stiff quark matter, that is to say, ultra-dense quark matter could still be non - conformal, being purely conformal at unrealistic densities, this means  $n_B \geq 40n_0$ .

We stress that the findings in Fig. 7 in this work are not the only ones in disagreement with those of Ref. [52]. Other works that appeared along the last year performing more general (mostly Bayesian) investigations of this conformality parameter  $d_c$  slightly and strongly disagree with Ref. [52]. They found the range of values  $0.1 \lesssim d_c \lesssim 0.45$  for their calculations. In particular, they pointed out [65, 66, 90, 91] (through studies with nucleonic or hybrid models) that  $d_c$  should be carefully interpreted. For instance, some of these robust explorations (e.g. Ref. [91] within the so-called extended Nambu–Jona-Lasinio model) always found  $d_c > 0.2$  with/without adjustment to converge to pQCD at high densities. Unfortunately, none of these works considered the presence of strong transitions possibly giving  $d_c \sim 1$ , as in here.

On the other hand, the discontinuities present in  $\Delta = \Delta(\epsilon)$ ,  $\Delta = \Delta(\mu_B)$ ,  $d_c = d_c(n_B/n_0)$  around the transition point lead us to hypothesize the following behavior for the QCD strong coupling since until no full QCD solu-

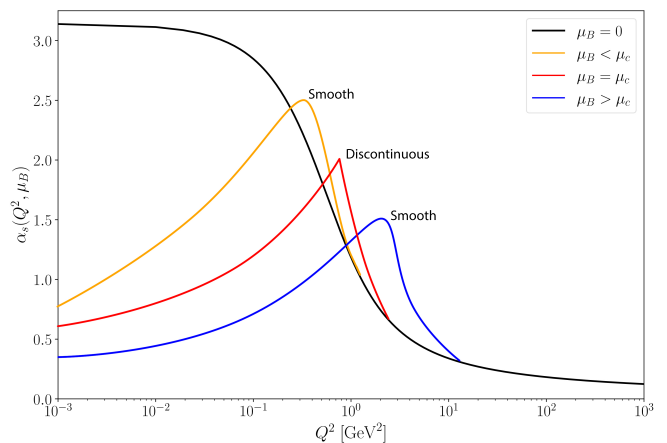


FIG. 8. Schematic representation for the behavior of the QCD strong coupling in a dense medium,  $\alpha_s(Q^2, \mu_B)$  (also depending on the energy-momentum scale  $Q^2$ ) inferred from  $\Delta$ . The black curve for the vacuum ( $\mu_B \neq 0$ ) case was obtained from Eq. (1) of Ref. [93]. The other curves represent our hypothesized behavior for ‘ $\alpha_s$ ’ before ( $\mu_B < \mu_c$ ), at ( $\mu_B = \mu_c$ ), and after ( $\mu_B > \mu_c$ ) the first-order phase transition occurs.

tion is known. Since Eq. (9) is tightly connected with the behavior of  $\beta_{\text{QCD}}$ , or more specifically, to  $\alpha_s$  (assuming the chiral condensates contribute more or less as constants). In this sense, it is reasonable to infer discontinuities present in the dense trace anomaly come from discontinuities in  $\alpha_s$  at the critical baryochemical potential. We sketch in Fig. 8 our proposal for  $\alpha_s$  in deep infrared energies. One can see lower values of  $\alpha_s$  at increasing  $\mu_B$  with a smooth maximum-like point (note the log scale) with  $\beta_{\text{QCD}} = 0$ , i.e.  $\Delta = 0$  in agreement with our twin-star results. Then, at the discontinuous phase-transition critical  $\mu_c$ , it displays a fully discontinuous behavior ( $\partial\alpha_s/\partial\mu_B(\mu_B \rightarrow \mu_c^+) \neq \partial\alpha_s/\partial\mu_B(\mu_B \rightarrow \mu_c^-)$ ) (see related recent studied in Ref. [92]). At higher densities ( $\mu_B > \mu_c$ ), it keeps decreasing as a whole with a smooth maximum (again with  $\beta_{\text{QCD}} = 0$ ). We put the results for  $\alpha_s$  in vacuum for comparison [93]. It is worth to mention that the distinct values of  $\alpha_s$  around  $Q^2 \sim 10^{-3} \text{ GeV}^2$  depend upon the infrared scenarios, e.g. the *decoupling* and *scaling* ones [93, 94].

We stress that similar (continuous) findings were obtained from effective models in the past (see, e.g. Refs. [95–97]) for increasing temperatures. At  $\mu_B \neq 0$ , we are not aware of similar non - perturbative studies for which we believe it is necessary a detail study. For instance, studies in vacuum within the functional-renormalization group, Schwinger-Dyson and machine learning (based upon experimental data) [93, 98] of the strong coupling at very low transferred momentum are known. Of course, our hypothesis could only be verified if future LQCD calculations at finite baryon densities (e.g. within quantum computing approaches [60]) are able to find first-order transition features, in particular,  $\alpha_s(Q^2, \mu_B)$ , as occur at finite temperatures [5, 6].

## VI. CONCLUSIONS AND OUTLOOK

We performed a comprehensive analysis of the dense QCD matter (normalized) trace anomaly,  $\Delta$ , at the interior of twin NSs (characterized by having sizeable cores of QM). Within the four categories of twin stars explored with rapid and slow boundary conditions in the radial pulsation equations, we found that their  $\Delta$  show an abrupt decreasing trend to negative values at intermediate densities after onset of QM. This is in contrast to being always positive at finite temperatures [5, 6], but with a similar trend at finite isospin densities [11].

We also discovered strong suggestions that for twin stars to exist in nature, the trace anomaly of intermediate density QCD matter has to be negative, at least, at the cores of these stars having ultradense central energy densities. This is due to the well known fact that twin stars require a stiff QM EoS, which tends to abruptly approach negative values for the trace anomaly leading. In particular, we were only able to find two stellar stable configurations with  $c_{s,Q}^2 = 0.5$ , one for Category I and another for Category IV, while the remaining families require  $c_{s,Q}^2 = 1$ , in the rapid scenario. All these differences with past studies come from the presence of a strong discontinuous phase transition representing the deconfinement transition.

It is worth mentioning that our results go into the opposite direction of Ref. [33], where they conjecture  $\Delta \geq 0$  at all NS densities. Interestingly, our findings slightly agree with Ref. [62], where they allowed  $\Delta$  to be generically negative at NS cores, but not too negative values and smoothly/slowly approaching conformality. Another fundamental difference with this and current works comes from noticing that the decrease behavior of  $\Delta$  in twin stars is steeply abrupt, i.e. large negative slopes, which directly depends on the stiffness of the QM EoS, i.e. on the value of the speed of sound squared, with higher values of  $c_{s,Q}^2$  leading to a steeper slope.

We also found that the presence of strong transitions modify highly non-trivially expectations for the behavior of the normalized pressures  $P/P_{SB}$  and the conformal factor  $d_c$  (being tightly related to  $\Delta$ ), in particular, large values for both,  $P/P_{SB} > 1$  and  $d_c > 0.6$ . Besides, the well-known band of Komoltsev-Kurkela was proven to be insufficient when applied to twin stars lying about its maximal region of  $n_B = 10n_0$  insured to be connected to pQCD at  $40n_B$ . We believe that more delicate studies of these aforementioned quantities must be redone explicitly including strong transitions by, e.g. employing recent parametric representations of the NS EoS allowing strong discontinuities from a phase transition [99]. Another similar research direction could extend these Bayesian studies to include sequential phase transitions, i.e. two strong discontinuities [100], which from all our figure above seem to be a reasonable mechanism to approach pQCD, even having large  $P/P_{SB}$  and ‘ $d_c$ ’.

Although there are some recent works (see, e.g. Ref. [101]) stating that twin stars are rare in nature, there

are still several microphysics unknowns relevant to build a fully appropriate twin star EoS. For instance, this last study of Ref. [101] within a fully dynamical general-relativistic framework does not take into account at any moment the phase conversion dynamics between hadronic matter and QM, then leading to the rapid and slow conditions [77] in the quasi-stationary limit.

On the other hand, we hypothesized that the existence of discontinuities in  $\Delta$  come from fundamental discontinuities in  $\beta_{QCD}$ , which in turn are manifested in  $\alpha_s(Q^2, \mu_B)$ , where non-perturbative QCD physics could be manifested through these discontinuities. Currently, estimates of this coupling are obtained in vacuum, inferring a smooth behavior in the infrared limit [93, 98].

We leave as future work detailed investigations concerning different thermodynamic constructions [12] at the transition point, non-equilibrium effects in the junction conditions [102] (both at the transition point), anisotropy modifications [103]. Besides, it would be worth to investigate the effects of the recent proposal of Ref. [104] for an averaged (squared) speed of sound, generalizing the Seidov’s criterion from twin stars.

## ACKNOWLEDGMENTS

The authors thank Tyler Gorda and Ryan Abbott for sharing data of Refs. [55] and [11], respectively. This work was partially supported by INCT-FNA (Process No. 464898/2014-5). V.P.G. and L.L. acknowledges support from CNPq, CAPES (Finance Code 001), and FAPERGS. V.P.G. was partially supported by the CAS President’s International Fellowship Initiative (Grant No. 2021VMA0019). J.C.J. is supported by Conselho Nacional de Desenvolvimento Científico e Tecnológico (CNPq) with Grant No. 151390/2024-0.

## APPENDIX A: TRACE ANOMALY OF HOLOGRAPHIC QUARK MATTER

Some years ago, the authors of Ref. [34] found a tentative result for the trace anomaly of dense matter applying the AdS/CFT duality, giving them

$$\epsilon = 3P + \frac{\sqrt{3}m^2}{2\pi}\sqrt{P}, \quad (36)$$

with  $m \approx 308.55$  MeV. Unfortunately, the way this equation was given is not very useful for our purposes. Thus, we manipulate it algebraically, obtaining

$$P = \frac{\epsilon}{3} + \frac{m^4}{24\pi^2} \pm \frac{\sqrt{3}m^2}{36\pi} \sqrt{12\epsilon + \frac{3m^4}{4\pi^2}} = P(\epsilon).$$

The ambiguity of the signs is solved by making this result consistent with the original one, i.e.

$$\epsilon - 3P = \frac{\sqrt{3}m^2}{2\pi}\sqrt{P} = -\frac{m^4}{8\pi^2} \mp \frac{\sqrt{3}m^2}{12\pi} \sqrt{12\epsilon + \frac{3m^4}{4\pi^2}} > 0,$$

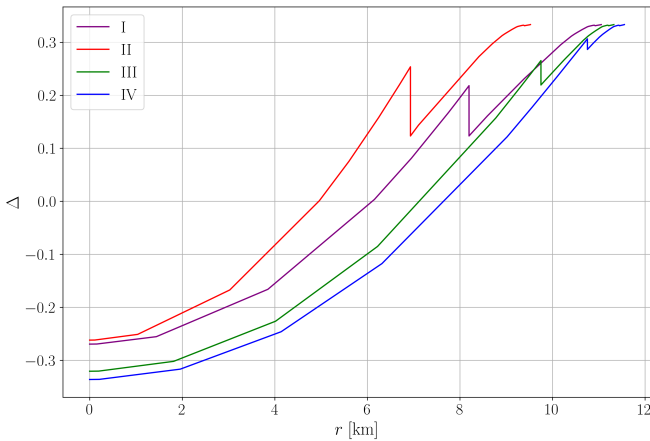


FIG. 9. Radial profiles of the dense trace anomaly for maximally-stable rapid twin stars obtained from the parameters listed in Table I. Notice the pronounced peaks at fixed radii for each category characterizing the phase-transition point. These curves were obtained from  $\Delta(r) = 1/3 - P_{\max}(r)/\epsilon_{\max}(r)$ , where  $\{P_{\max}, \epsilon_{\max}\}$  are solutions of the TOV equations for the maximal-mass twin stars.

implying the need of a negative sign in  $P = P(\epsilon)$  above. It is worth to also remark that this choice agrees with one boundary condition of the TOV equations, which need  $P = 0$  for a given energy density. A positive sign would spoil this condition, producing stars with unrealistic radii.

#### APPENDIX B: ROBUSTNESS OF THE POLYTROPIC MODEL FOR NUCLEAR MATTER IN $\Delta$

As mentioned in Sec. V, we prove that even using a polytropic model allows  $\Delta < 0$  at intermediate densities.

It is known that for a given polytrope ‘ $i$ ’ within a set of piecewise polytropic pressures, one has

$$P_{\text{poly}} = \kappa_i n^{\Gamma_i}, \quad \epsilon_{\text{poly}} = \frac{\kappa_i n^{\Gamma_i}}{(\Gamma_i - 1)} + m_0 n,$$

for the pressure and energy density, respectively, with ‘ $m_0$ ’ the particle’s mass,  $n$  particle’s density, and  $\Gamma$  polytropic index. This result was obtained by using  $P = n^2 d(\epsilon/n)/dn$ . Thus, the (unnormalized) polytropic dense trace anomaly is

$$[T_{\mu}^{\mu}]_{\text{poly}} = \epsilon_{\text{poly}} + 3(\epsilon_{\text{poly}} - m_0 n)(1 - \Gamma_i).$$

Interestingly, notice that in the limit of  $\epsilon_{\text{poly}} \gg m_0 n$ , i.e. somewhat high densities or equivalently intermediate QCD densities, one gets

$$[T_{\mu}^{\mu}]_{\text{poly}} = \epsilon_{\text{poly}} (1 + 3(1 - \Gamma_i)) = 3\epsilon_{\text{poly}} \left( \frac{4}{3} - \Gamma_i \right),$$

or also equivalently for the normalized case

$$\Delta_{\text{poly}} = \frac{[T_{\mu}^{\mu}]_{\text{poly}}}{3\epsilon_{\text{poly}}} = \frac{4}{3} - \Gamma_i. \quad (37)$$

In other words,  $[T_{\mu}^{\mu}]_{\text{poly}} < 0$  (or  $\Delta_{\text{poly}} < 0$ ) when  $\Gamma_i > 4/3$ . In other words, all works in the literature (see e.g. Refs. [21, 29] surpassing  $\Gamma = 4/3$ ) employing polytropes at intermediate ‘ $n$ ’ will probe negative  $[T_{\mu}^{\mu}]_{\text{poly}}$ . Besides, notice that at intermediate densities  $P \approx \epsilon$ , then the corresponding (squared) speed of sound behaves as

$$c_s^2 = \frac{\Gamma_i P}{\epsilon + P} \approx \frac{\Gamma_i}{2}.$$

Thus,  $\Gamma_i > 4/3$  implies  $c_s^2 > 2/3 \approx 0.67$ , i.e.  $[T_{\mu}^{\mu}]_{\text{poly}} < 0$  occurs for large squared speeds of sound ( $> 0.5$ ).

Of course, one can make  $[T_{\mu}^{\mu}]_{\text{poly}}$  positive again by adding an ultra-dense EoS, e.g. the bag model (or pQCD like Ref. [29]) for which  $[T_{\mu}^{\mu}]_{\text{bag}} = 4B$  (‘ $B$ ’ being the bag constant), one gets

$$[T_{\mu}^{\mu}]_{\text{poly}} + [T_{\mu}^{\mu}]_{\text{MIT}} = 3\epsilon_{\text{poly}} \left( \frac{4}{3} - \Gamma_i \right) + 4B,$$

which can make the total trace anomaly to be positive.

#### APPENDIX C: RADIAL PROFILES FOR THE TWIN-STAR TRACE ANOMALIES

Apart from our main results, one can also be interested in the values reached by  $\Delta$  at the core of twin stars. In order to answer that question, we show in Fig. 9 the radial profiles for the twin star trace anomalies for the same of four EoSs (one for each category) of Table I considering only rapid conversions. In particular, we chose to display only our findings of the trace anomaly inside the maximum-mass twin stars for simplicity. This configuration is also the last one with a positive fundamental eigenfrequency, i.e. the last stable one. Finally, we verified that other rapid-conversion (as well as slow-conversion) twin stars show basically the same behavior as the maximally-stable twin star.

#### APPENDIX D: RESULTS FOR TWIN-STAR TRACE ANOMALIES WITH INTERMEDIATE CET EOS

It is worth to test if our main conclusions for the twin star trace anomaly are still true when using the intermediate CET EoS of Ref. [21] with the following agnostic GPP parametrization:  $\log_{10}[\rho_0/(g \text{ cm}^{-3})] = 13.865$ ,  $\log_{10} K_1 = -27.22$ ,  $\Gamma_1 = 2.748$ ,  $\Gamma_2 = 6.5$  and  $\Gamma_3 = 3.25$ . Since this hadronic EoS is not as stiff as the one employed along this work, we found a significant smaller

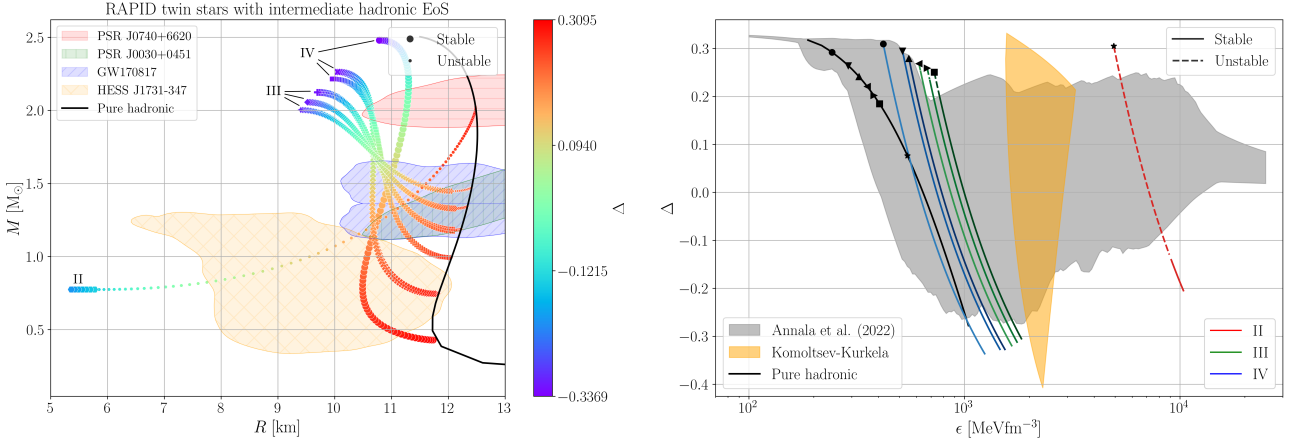


FIG. 10. Same captions and constraints as in Fig. 3 but for all rapid twin stars employing the intermediate CET EoS in the hadronic sector. Note that one gets again the sudden decrease of  $\Delta$  although still in agreement with the band of Annala et al. (2022) [20] except the rightmost curve being marginally stable (see also the leftmost  $M$ - $R$  relation in the left panel).

number of twin-star EoSs that satisfy the two-solar mass constraint. Thus, we found that twin stars in Category I are not possible to exist due to the lack of stiffness in the intermediate CET hadronic EoS. On the other hand, we present in Fig. 10 our predictions for all remaining categories with rapid-conversion junction conditions (where the usual stability criterion,  $\partial M/\partial \epsilon_c \geq 0$  works) for the  $M$ - $R$  relation (left panel) and the trace anomaly as function of energy density (right panel), following the same color scheme as previous figures in the main text. Results for slow junction conditions are consistent to those presented in the main text, i.e. only Category II configurations present a larger number of valid EoSs when compared to the rapid scenario.

### APPENDIX E: PROOFS ABOUT THE CONSTANT-SPEED-OF-SOUND MODEL

We pass to prove Eq. (33) from Eq. (31). First, we obtain the corresponding energy density using known thermodynamic relations

$$\begin{aligned} \epsilon_Q &= -P_Q + \mu_B n_B^Q = \\ &N(\mu_B)\gamma\mu_B^{\gamma+1} + \left(\frac{\gamma-1}{2}\right)C(\mu_B)\mu_B^{(1+\gamma)/2} + \\ &\left(\frac{\partial N}{\partial \ln \mu_B}\right)\mu_B^{1+\gamma} + \left(\frac{\partial C}{\partial \ln \mu_B}\right)\mu_B^{(1+\gamma)/2} + B, \end{aligned}$$

being appropriately rewritten as (generically with  $N = N(\mu_B)$  and  $C = C(\mu_B)$ )

$$\begin{aligned} &\left(N\gamma + \frac{\partial N}{\partial \ln \mu_B}\right)\mu_B^{\gamma+1} + \\ &\left[\left(\frac{\gamma-1}{2}\right)C + \frac{\partial C}{\partial \ln \mu_B}\right]\mu_B^{(1+\gamma)/2} - (\epsilon_Q - B) = 0, \end{aligned}$$

where we pass to define  $N_r \equiv N + (1/\gamma)(\partial N/\partial \ln \mu_B)$  and  $C_r \equiv C + [2/(\gamma-1)](\partial C/\partial \ln \mu_B)$  as *running* generalizations. This equation can be identified with a 2nd-order algebraic one with  $x \equiv \mu_B^{(1+\gamma)/2}$ , thus giving two real roots given by

$$\begin{aligned} \mu_B^{(1+\gamma)/2} &= -\left(\frac{\gamma+1}{\gamma}\right)\frac{C_r}{4N_r} \\ &\pm \left(\frac{C_r}{4N_r}\right)\sqrt{\left(\frac{\gamma-1}{\gamma}\right)^2 + \frac{16N_r}{\gamma C_r^2}(\epsilon - B)}. \end{aligned}$$

This last result must be introduced in Eq. (31), reordered and simplified to finally give Eq. (33). For the same reasons discussed in Appendix A and footnote 6, we chose the negative sign in the above solutions for ‘ $x$ ’.

On the other hand, leaving aside the CSS parametrization with  $c_s^2 = \text{constant} = 1/\gamma$ , one interesting effect happens within our results above. In particular, let us consider that ‘ $\gamma$ ’ and  $c_s^2$  are independent quantities, i.e.  $c_{s,Q}^2 \neq 1/\gamma$ , with  $c_s^2 = dP/d\epsilon$ . Now, fixing  $N = \text{constant}$ , ‘ $C$ ’ running and  $\gamma = 1$ , we get

$$\mu_B = \sqrt{\frac{\epsilon - B}{N}} \text{ or } \ln \mu_B = (1/2)\ln[(\epsilon - B)/N],$$

which after being introduced in Eq. (33) gives

$$P_Q = \epsilon_Q - 2B \pm \sqrt{\frac{\epsilon_Q - B}{N}} \left( C + \lim_{\gamma \rightarrow 1} \frac{1}{\gamma - 1} \frac{\partial C}{\partial \ln \mu_B} \right)$$

or more appropriately

$$\begin{aligned} P_Q &= \epsilon_Q - 2B \\ &\pm \sqrt{\frac{\epsilon_Q - B}{N}} \left( C + \lim_{\gamma \rightarrow 1} \frac{2}{\gamma - 1} \frac{\partial C}{\partial \ln(\epsilon_Q/N)} \right). \end{aligned}$$

Thus, assuming a running non-zero condensation term makes to diverge the EoS as  $\gamma \rightarrow 1$  (also its  $c_s^2$ ) coming



from a fast increment in the running behavior of ‘ $C$ ’. If one assumes it is constant, then the appropriate choice of sign would be minus in order to not surpass the causality limit ( $c_s^2 = 1$ ) at high energy densities. In any case, something is evident for a generic  $\gamma < 1$ : *large values*

*for the speeds of sound at intermediate densities point to being related to strong effects from the non - perturbative condensation term, which commonly only enters as subdominant terms, for instance, in CFL quark matter.*

- 
- [1] B. L. Ioffe, V. S. Fadin and L. N. Lipatov, *Quantum Chromodynamics: Perturbative and Nonperturbative Aspects* (Cambridge University Press, New York, 2010).
- [2] T. Gehrmann and B. Malaescu, *Ann. Rev. Nucl. Part. Sci.* **72**, 233 (2022).
- [3] J. Barata, A. V. Sadofyev and X. N. Wang, *Phys. Rev. D* **107**, L051503 (2023).
- [4] J. I. Kapusta and C. Gale, *Finite-temperature field theory: Principles and applications* (Cambridge University Press, New York, 2006).
- [5] A. Bazavov, T. Bhattacharya, M. Cheng, N. H. Christ, C. DeTar, S. Ejiri, S. Gottlieb, R. Gupta, U. M. Heller and K. Huebner, *et al.* *Phys. Rev. D* **80**, 014504 (2009)
- [6] S. Borsanyi, Z. Fodor, C. Hoelbling, S. D. Katz, S. Krieg and K. K. Szabo, *Phys. Lett. B* **730**, 99 (2014)
- [7] G. S. Bali, F. Bruckmann, G. Endrodi, Z. Fodor, S. D. Katz, S. Krieg, A. Schafer and K. K. Szabo, *JHEP* **02**, 044 (2012)
- [8] B. B. Brandt, F. Cuteri, G. Endrödi, G. Markó, L. Sandbote and A. D. M. Valois, *JHEP* **11**, 229 (2023)
- [9] G. Endrodi and G. Marko, *Phys. Rev. D* **109**, 034506 (2024)
- [10] B. B. Brandt, F. Cuteri and G. Endrodi, *JHEP* **07**, 055 (2023)
- [11] R. Abbott *et al.* [NPLQCD], *Phys. Rev. D* **108**, 114506 (2023)
- [12] N. K. Glendenning, *Compact Stars – Nuclear Physics, Particle Physics and General Relativity* (Springer, New York, 2000).
- [13] K. Nagata, *Prog. Part. Nucl. Phys.* **127** (2022), 103991
- [14] E. Fonseca *et al.*, *Astrophys. J.* **832**, 167 (2016)
- [15] M. Linares, T. Shahbaz and J. Casares, *Astrophys. J.* **859**, 54 (2018)
- [16] M. Miller *et al.*, *Astrophys. J. Lett.* **887**, L24 (2019)
- [17] T. E. Riley *et al.*, *Astrophys. J. Lett.* **887**, L21 (2019)
- [18] H. T. Cromartie *et al.*, *Nature Astron.* **4**, no.1, 72 (2019)
- [19] B. P. Abbott *et al.* [LIGO Scientific and Virgo], *Phys. Rev. Lett.* **119**, 161101 (2017)
- [20] E. Annala, T. Gorda, E. Katerini, A. Kurkela, J. Nättilä, V. Paschalidis and A. Vuorinen, *Phys. Rev. X* **12**, 011058 (2022)
- [21] K. Hebeler, J. Lattimer, C. Pethick and A. Schwenk, *Astrophys. J.* **773**, 11 (2013)
- [22] A. Kurkela, P. Romatschke and A. Vuorinen, *Phys. Rev. D* **81**, 105021 (2010)
- [23] A. Sorensen *et al.*, *Prog. Part. Nucl. Phys.* **134**, 104080 (2024).
- [24] C. Ratti, *Rept. Prog. Phys.* **81**, 084301 (2018)
- [25] R. Somasundaram, I. Tews and J. Margueron, *Phys. Rev. C* **107**, 025801 (2023)
- [26] I. Tews, J. Carlson, S. Gandolfi and S. Reddy, *Astrophys. J.* **860**, 149 (2018)
- [27] A. Cherman, T. D. Cohen and A. Nellore, *Phys. Rev. D* **80**, 066003 (2009)
- [28] P. Bedaque and A. W. Steiner, *Phys. Rev. Lett.* **114**, 031103 (2015)
- [29] E. Annala, T. Gorda, A. Kurkela, J. Nättilä and A. Vuorinen, *Nature Phys.* **16**, 907-910 (2020) [[arXiv:1903.09121](https://arxiv.org/abs/1903.09121) [astro-ph.HE]].
- [30] R. Somasundaram, I. Tews and J. Margueron, *Phys. Rev. C* **107**, L052801 (2023)
- [31] O. Komoltsev, R. Somasundaram, T. Gorda, A. Kurkela, J. Margueron and I. Tews, *Phys. Rev. D* **109**, 094030 (2024)
- [32] L. Brandes, W. Weise and N. Kaiser, *Phys. Rev. D* **107**, 014011 (2023)
- [33] Y. Fujimoto, K. Fukushima, L. D. McLerran and M. Praszalowicz, *Phys. Rev. Lett.* **129**, 252702 (2022).
- [34] C. Hoyos, D. Rodríguez Fernández, N. Jokela and A. Vuorinen, *Phys. Rev. Lett.* **117**, 032501 (2016)
- [35] L. D. Landau, E. M. Lifshitz, *The Classical Theory of Fields, 4th ed., Course of Theoretical Physics*, vol. 2 (Butterworth-Heinemann, Oxford, 1987).
- [36] Z. Y. Lu, C. J. Xia and M. Ruggieri, *Eur. Phys. J. C* **80**, 46 (2020)
- [37] V. Vovchenko, B. B. Brandt, F. Cuteri, G. Endrödi, F. Hajkarim and J. Schaffner-Bielich, *Phys. Rev. Lett.* **126**, 012701 (2021)
- [38] M. Albright and J. I. Kapusta, *Phys. Rev. C* **93**, 014903 (2016)
- [39] D. Kharzeev and K. Tuchin, *JHEP* **09**, 093 (2008)
- [40] L. D. Landau, E. M. Lifshitz, *Fluid Mechanics, 2nd ed., Course of Theoretical Physics*, vol. 6 (Butterworth-Heinemann, Oxford, 1987).
- [41] P. Haensel, A. Y. Pothekin, and D. G. Yakovlev, *Neutron Stars 1* (Springer-Verlag, New York, 2007).
- [42] A. Cherman, T. Jacobson, S. Sen and L. G. Yaffe, *Phys. Rev. D* **102**, 105021 (2020)
- [43] A. Cherman, S. Sen and L. G. Yaffe, *Phys. Rev. D* **100**, 034015 (2019)
- [44] F. E. Canfora, D. Dudal, I. F. Justo, P. Pais, L. Rosa and D. Vercauteren, *Eur. Phys. J. C* **75**, 326 (2015)
- [45] P. Jakobus, A. Motornenko, R. O. Gomes, J. Steinheimer and H. Stoecker, *Eur. Phys. J. C* **81**, 41 (2021)
- [46] A. Grozin, *Int. J. Mod. Phys. A* **28**, 1350015 (2013)
- [47] M. Rho, *Symmetry* **14**, 2154 (2022)
- [48] D. E. Alvarez-Castillo, D. B. Blaschke, A. G. Grunfeld and V. P. Pagura, *Phys. Rev. D* **99**, 063010 (2019)
- [49] A. Zacchi, M. Hanauske and J. Schaffner-Bielich, *Phys. Rev. D* **93**, 065011 (2016)
- [50] A. Zacchi, L. Tolos and J. Schaffner-Bielich, *Phys. Rev. D* **95**, 103008 (2017)
- [51] D. E. Alvarez-Castillo and D. B. Blaschke, *Phys. Rev. C* **96**, 045809 (2017)
- [52] E. Annala, T. Gorda, J. Hirvonen, O. Komoltsev, A. Kurkela, J. Nättilä and A. Vuorinen, *Nature Commun.* **14**, 8451 (2023)

- [53] L. Brandes, W. Weise and N. Kaiser, Phys. Rev. D **108**, 094014 (2023)
- [54] L. Brandes and W. Weise, Symmetry **16**, 111 (2024)
- [55] T. Gorda, K. Hebeler, A. Kurkela, A. Schwenk and A. Vuorinen, Astrophys. J. **955**, 100 (2023)
- [56] J. E. Christian, J. Schaffner-Bielich and S. Rosswog, Phys. Rev. D **109**, 063035 (2024)
- [57] J. J. Li, A. Sedrakian and M. Alford, Astrophys. J. **967**, 116 (2024)
- [58] S. Blacker and A. Bauswein, [[arXiv:2406.14669](#) [astro-ph.HE]].
- [59] S. Hensh, Y. J. Huang, T. Kojo, L. Baiotti, K. Takami, S. Nagataki and H. Sotani, [[arXiv:2407.09446](#) [astro-ph.HE]].
- [60] A. Yamamoto, PoS **LATTICE2021**, 122 (2021)
- [61] E. Lope-Otero and A. Wojnar, [[arXiv:2402.03914](#) [gr-qc]].
- [62] C. Ecker and L. Rezzolla, Mon. Not. Roy. Astron. Soc. **519**, 2615-2622 (2022)
- [63] B. J. Cai, B. A. Li and Z. Zhang, Phys. Rev. D **108**, 103041 (2023)
- [64] B. J. Cai and B. A. Li, [[arXiv:2406.05025](#) [astro-ph.HE]].
- [65] J. Takatsy, P. Kovacs, G. Wolf and J. Schaffner-Bielich, Phys. Rev. D **108**, 043002 (2023)
- [66] M. Albino, T. Malik, M. Ferreira and C. Providência, [[arXiv:2406.15337](#) [nucl-th]].
- [67] W. Zhou, H. Shen, J. Hu and Y. Zhang, Phys. Rev. D **110**, 043017 (2024)
- [68] Y. Fujimoto, K. Fukushima, K. Hotokezaka and K. Kyutoku, [[arXiv:2408.10298](#) [astro-ph.HE]].
- [69] M. F. O'Boyle, C. Markakis, N. Stergioulas and J. S. Read, Phys. Rev. D **102**, 083027 (2020)
- [70] G. Lugones, M. Mariani and I. F. Ranea-Sandoval, JCAP **03**, 028 (2023)
- [71] V. P. Goncalves and L. Lazzari, Eur. Phys. J. C **82**, no.4, 288 (2022)
- [72] M. G. Alford, S. Han and M. Prakash, Phys. Rev. D **88**, 083013 (2013)
- [73] J. E. Christian, A. Zacchi and J. Schaffner-Bielich, Eur. Phys. J. A **54**, 28 (2018)
- [74] O. Komoltsev and A. Kurkela, Phys. Rev. Lett. **128**, 202701 (2022)
- [75] D. Gondek, P. Haensel and J. Zdunik, Astron. Astrophys. **325**, 217 (1997)
- [76] P. Haensel, J. L. Zdunik and R. Schaeffer, Astronomy and Astrophysics **217**, 137 (1989)
- [77] J. P. Pereira, C. V. Flores and G. Lugones, Astrophys. J. **860**, 12 (2018)
- [78] J. C. Collins, A. Duncan and S. D. Joglekar, Phys. Rev. D **16**, 438-449 (1977)
- [79] N. K. Nielsen, Nucl. Phys. B **120**, 212-220 (1977)
- [80] B. P. Abbott *et al.* [LIGO Scientific and Virgo], Phys. Rev. Lett. **121**, 161101 (2018)
- [81] V. Doroshenko *et al.*, Nature Astron. **6**, 1444-1451 (2022).
- [82] M. Mariani, I. F. Ranea-Sandoval, G. Lugones and M. G. Orsaria, [[arXiv:2407.06347](#) [astro-ph.HE]].
- [83] T. Gorda, O. Komoltsev, A. Kurkela and A. Mazeliauskas, JHEP **06**, 002 (2023)
- [84] C. Providência, T. Malik, M. B. Albino and M. Ferreira, [[arXiv:2307.05086](#) [nucl-th]].
- [85] J. C. Jiménez and E. S. Fraga, Phys. Rev. D **100**, 114041 (2019)
- [86] R. Chiba and T. Kojo, Phys. Rev. D **109**, 076006 (2024)
- [87] C. Zhang and R. B. Mann, Phys. Rev. D **103**, 063018 (2021)
- [88] C. Vasquez Flores and G. Lugones, Phys. Rev. D **82**, 063006 (2010)
- [89] M. Alford, M. Braby, M. W. Paris and S. Reddy, Astrophys. J. **629**, 969-978 (2005)
- [90] T. Malik, V. Dexheimer and C. Providência, [[arXiv:2404.07936](#) [nucl-th]].
- [91] K. D. Marquez, T. Malik, H. Pais, D. P. Menezes and C. Providência, [[arXiv:2407.18452](#) [nucl-th]].
- [92] I. Y. Aref'eva, A. Hajilou, P. Slepov and M. Usova, [[arXiv:2407.14448](#) [hep-th]].
- [93] A. Deur, S. J. Brodsky and C. D. Roberts, Prog. Part. Nucl. Phys. **134**, 104081 (2024)
- [94] A. Deur, S. J. Brodsky and G. F. de Teramond, Nucl. Phys. **90**, 1 (2016)
- [95] F. M. Steffens, Braz. J. Phys. **36**, 582-585 (2006)
- [96] J. Braun and H. Gies, JHEP **06**, 024 (2006)
- [97] W. j. Fu, J. M. Pawlowski and F. Rennecke, Phys. Rev. D **101**, 054032 (2020)
- [98] X. Y. Wang, C. Dong and X. Liu, Chin. Phys. Lett. **41**, 031201 (2023)
- [99] L. Lindblom, Phys. Rev. D **110**, 043018 (2024)
- [100] M. G. Alford and A. Sedrakian, Phys. Rev. Lett. **119**, 161104 (2017)
- [101] M. Naseri, G. Bozzola and V. Paschalidis, [[arXiv:2406.15544](#) [astro-ph.HE]].
- [102] P. B. Rau and G. G. Salaben, Phys. Rev. D **108**, 103035 (2023)
- [103] D. Horvat, S. Ilijic and A. Marunovic, Class. Quant. Grav. **28**, 025009 (2011)
- [104] M. Marczenko, [[arXiv:2407.15486](#) [nucl-th]].